HOLTEC INTERNATIONAL

Holtec Technology Campus, One Holtec Blvd, Camden, NJ 08104
Telephone (856) 797-0900
Fax (856) 797-0909

May 28, 2021

U.S. Nuclear Regulatory Commission
ATTN: Document Control Desk
Washington, DC 20555-0001

Docket No. 99902086 - HDI Spent Fuel Pool Heatup Calculation Methodology

Subject: Response to Request for Additional Information - Holtec Spent Fuel Pool Heat Up Calculation Methodology Topical Report

References:

1. Letter from Holtec International to US NRC, "Holtec Spent Fuel Pool Heat Up Calculation Methodology Topical Report," September 29, 2020 (ML20280A524)

2. US NRC Electronic Mail Request to Andrea Sterdis (HDI) "Formal Transmittal of the US NRC Requests for Additional Information for Holtec Topical Report HI-2200750 Revision 0, "Holtec Spent Fuel Pool Heat Up Calculation Methodology," March 31, 2021 (ML21077A102)

Dear Sir or Madam:

In Reference 1, Holtec Decommissioning International, LLC (HDI) submitted a Topical Report providing a methodology for calculating Spent Fuel Pool heat up for NRC review and approval. Holtec believes the methodology will be a large benefit in reducing zirconium fire risks in the spent fuel pool.

In Reference 2, the NRC transmitted a request for additional information (RAI) concerning the Topical Report. The following Enclosures to this letter provide a response to the NRC RAI.

Enclosure 1 (submitted separately via the BOX) provides a proprietary version of the RAI response. This enclosure contains information proprietary to Holtec and is therefore supported by an affidavit signed by Holtec which is provided in Enclosure 3.

Enclosure 2 provides a non-proprietary, redacted version of the RAI response.

If you have any questions, please contact me at 856-797-0900 ext. 3813.

Sincerely,

Andrea Sterdis

Digitally signed by Andrea Sterdis
DN: cn=Andrea Sterdis, c=US, o=Holtec Decommissioning International, ou=HDI, email=a.sterdis@holtec.com
Date: 2021.05.28 16:24:25 -04'00'

Andrea L. Sterdis
VP, Regulatory and Environmental Affairs
Holtec Decommissioning International

HOLTEC INTERNATIONAL

Holtec Technology Campus, One Holtec Blvd, Camden, NJ 08104
Telephone (856) 797-0900
Fax (856) 797-0909

Enclosures:

Enclosure 1 (SUBMITTED SEPARATELY) Holtec Response to Request for Additional Information concerning Spent Fuel Pool Heat Up Calculation Methodology Topical Report (~~Holtec Proprietary Withhold Information from Public Disclosure pursuant to 10 CFR 2.390~~)

Enclosure 2 Holtec Responses to Request for Additional Information concerning Spent Fuel Pool Heat Up Calculation Methodology Topical Report (Non-Proprietary)

Enclosure 3 Affidavit Pursuant to 10 CFR 2.390 to Withhold Information from Public Disclosure

Enclosure 4 RAI 02, Reference 2.1 "Effective Thermal Conductivity and Edge Conductance Model for a Spent-Fuel Assembly

cc:
Robert Lucas, NRC, NRR/DORL/LLPB
Dennis Morey, NRC, NRR/DORL/LLPB
Ekaterina Lenning, NRC, NRR/DORL/LLPB
Christopher Regan, NRC, NMSS/DFM

Enclosure 1

Holtec Response to Request for Additional Information concerning Spent Fuel Pool Heat Up Calculation Methodology Topical Report

~~Proprietary Version~~

~~Withhold Information From Public Disclosure Under 10 CFR 2.390~~

(19 Pages Submitted Separately)

Enclosure 2

Holtec Response to Request for Additional Information concerning Spent Fuel Pool Heat Up Calculation Methodology Topical Report

Redacted Version

(19 Pages Attached)

RAI-01

Treatment of near-wall locations

[

[PROPRIETARY INFORMATION WITHHELD PER 10 CFR 2.390]

] 4.a, 4.b

Regulatory Justification	SRP Section 15.0.2, Subsection III.3c				
Associated Section	3.1.4 Initial and Boundary Conditions				
Level of Concern	2	Level of Impact	5	Level of Effort	3
Overall Significance	Medium				
Holtec Response	[**[PROPRIETARY INFORMATION WITHHELD PER 10 CFR 2.390]**] 4.a, 4.b Therefore, the methodology proposed by Holtec does improve the safety of the spent fuel storage.				

RAI-02

Lumped Analysis vs. Pin by Pin Analysis

[

[PROPRIETARY INFORMATION WITHHELD PER 10 CFR 2.390]

] **4.a, 4.b**

Regulatory Justification	SRP Section 15.0.2, Subsection III.3b				
Associated Section	3.3.1.4 Level of Detail in the Model				
Level of Concern	1	Level of Impact	3	Level of Effort	1
Overall Significance	High				
Holtec Response	**[** **[PROPRIETARY INFORMATION WITHHELD PER 10 CFR 2.390]** **]** **4.a, 4.b** The methodology in the main part of the report will be expanded as follows: **[** **[PROPRIETARY INFORMATION WITHHELD PER 10 CFR 2.390]** o				

[PROPRIETARY INFORMATION WITHHELD PER 10 CFR 2.390]

] **4.a, 4.b**

- The paper shows that the method is validated through measurements,

[PROPRIETARY INFORMATION WITHHELD PER 10 CFR 2.390]

] **4.a, 4.b**

- The approach is considered conservative due to the following reasons:

[

	[PROPRIETARY INFORMATION WITHHELD PER 10 CFR 2.390] **]** [4.a, 4.b] This is further discussed in the response to RAI-03.

	Reference for Response to RAI-02. [2.1] Manteufel, R.D. and N.E. Todreas, “Effective Thermal Conductivity and Edge Configuration Model for Spent Fuel Assembly,” Nuclear Technology, Vol. 105, pp. 421–440, March 1994.

RAI-03

Radial and Axial Peaking

[

[PROPRIETARY INFORMATION WITHHELD PER 10 CFR 2.390]

] 4.a, 4.b

Regulatory Justification	SRP Section 15.0.2, Subsection III.3b				
Associated Section	3.3.1.4 Level of Detail in the Model				
Level of Concern	2	Level of Impact	2	Level of Effort	1
Overall Significance	High				
Holtec Response	[**[PROPRIETARY INFORMATION WITHHELD PER 10 CFR 2.390]**] 4.a, 4.b (see for example the HI-STAR 100 Storage SAR [3.1],				

tables 2.1.3 and 2.1.4, and the SER on the initial submittal of this SAR [3.2], Section 4.3). **[**

[PROPRIETARY INFORMATION WITHHELD PER 10 CFR 2.390]

] **4.a, 4.b**

For PWR fuel, axial burnups were also extensively analyzed in support of Burnup Credit for spent fuel transportation casks, as documented in NUREG/CR-6801 [3.3], with results documented in Table 5 of that document. **[Proprietary Information Withheld Per 10 CFR 2.390.]** **4.a, 4.b** Note that for lower burnup, the NUREG reports slightly higher values, up to about 1.215 (for burnups between 14 and 18 GWd/mtU). **[Proprietary Information Withheld Per 10 CFR 2.390.]** **4.a, 4.b**

For BWR fuel, similar studies were performed and are documented in NUREG/CR-7224 [3.4]. For high burnup assemblies, results are shown in that NUREG in Figure 6.3, with maximum values generally no more than 1.2. **[**

[PROPRIETARY INFORMATION WITHHELD PER 10 CFR 2.390]

.

	[PROPRIETARY INFORMATION WITHHELD PER 10 CFR 2.390]

	[PROPRIETARY INFORMATION WITHHELD PER 10 CFR 2.390]

[PROPRIETARY INFORMATION WITHHELD PER 10 CFR 2.390]

] 4.a, 4.b

References for Response to RAI-03

[3.1] HI-STAR 100 Final Safety Analysis Report, Holtec Report HI-2012610, Rev. 0, March 2001
[3.2] NRC Safety Evaluation Report and CoC, Holtec HI-STAR 100 Cask System, April 1999
[3.3] "Recommendations for Addressing Axial Burnup in PWR Burnup Credit Analyses", NUREG/CR-6801, ORNL/TM–2001/273, Oak Ridge National Laboratory, March 2003.

	[3.4] "Axial Moderator Density Distributions, Control Blade Usage, and Axial Burnup Distributions for Extended BWR Burnup Credit", NUREG/CR-7224, ORNL/TM-2015/544, Oak Ridge National Laboratory, August 2016. [3.5] "Horizontal Burnup Gradient Datafile for PWR Assemblies", DOE/RW-0496, Office of Civilian Radioactive Waste Management, May 1997. [3.6] Westinghouse Technology Systems Manual, Section 2.2, Power Distribution Limits, USNRC HRTD, Rev. 0508, ML11223A208

RAI-04

Time Step Sensitivity

[

[PROPRIETARY INFORMATION WITHHELD PER 10 CFR 2.390]

] 4.a, 4.b

Regulatory Justification	SRP Section 15.0.2, Subsection III.3d, Appendix K to 10 CFR 50, and *TMI {Three Mile Island] action items for PWR*				
Associated Section	3.3.2.1 Numerical Solutions & 3.3.5.4 Sensitivity Studies				
Level of Concern	3	Level of Impact	3	Level of Effort	4
Overall Significance	Low				
Holtec Response	[**[PROPRIETARY INFORMATION WITHHELD PER 10 CFR 2.390]**] 4.a, 4.b [<table><tr><td></td><td></td></tr><tr><td></td><td></td></tr><tr><td></td><td></td></tr><tr><td></td><td></td></tr><tr><td></td><td></td></tr><tr><td></td><td></td></tr><tr><td></td><td></td></tr><tr><td></td><td></td></tr></table> 4.a, 4.b				

RAI-05

Planar Surface Area

[

[PROPRIETARY INFORMATION WITHHELD PER 10 CFR 2.390]

]4.a, 4.b

Regulatory Justification	SRP Section 15.0.2, Subsection III.3e				
Associated Section	3.3.5.1 Important Sources of Uncertainty				
Level of Concern	3	Level of Impact	3	Level of Effort	4
Overall Significance	Low				
Holtec Response	[**[PROPRIETARY INFORMATION WITHHELD PER 10 CFR 2.390]**]4.a, 4.b				

RAI-06

Uncertainty due to emissivity

[

[PROPRIETARY INFORMATION WITHHELD PER 10 CFR 2.390]

]4.a, 4.b

Regulatory Justification	SRP Section 15.0.2, Subsection III.3e				
Associated Section	3.3.5.1 Important sources of Uncertainty				
Level of Concern	3	Level of Impact	3	Level of Effort	3
Overall Significance	Low				
Holtec Response	Surface emissivities are significantly affected by surface layers on the cladding (crud usually increases emissivity); therefore, the assumed oxidation layer and any exposed zircaloy surfaces are assumed to have the emissivity resulting from MATPRO Equation 4.1-8 [2] (equal to 0.8 or higher) using the oxidation thicknesses from [1]. Furthermore, Table B-3.II of [2] also shows an emissivity of fuel cladding with crud well over 0.8. Therefore, use of an emissivity of 0.8 for zircaloy cladding is conservative. Emissivity of stainless-steel plates that are used for the rack cell walls is 0.587 per ORNL studies [3] and [4]. The variation in emissivity of stainless-steel with temperature is extremely small (~ 0.05) in large temperature range as shown in reference [5]. Moreover, it must be noted that the emissivity values of 0.8 and 0.587 for zircaloy cladding and stainless-steel plates, respectively, have been approved by USNRC in multiple Holtec's dry storage applications (USNRC Docket Nos. 72-1014, 72-1032, 72-1040, 71-9325, 71-9367, 71-9373, 71-9374, etc.). NRC staff further mentions in their SERs (Section 3.2 on Docket Nos. 71-9367, 71-9374) that the material properties and surface emissivities used in these applications are acceptable.				

	The variances in emissivity can alter the radiation heat transfer characteristics of the surfaces and therefore change the peak cladding temperatures. However, as noted in Section 4.2.7 of [1], the impact of emissivity variations on the peak cladding temperature (PCT) is extremely small. As a defense-in-depth, Holtec also performed sensitivity evaluations **[** **[PROPRIETARY INFORMATION WITHHELD PER 10 CFR 2.390]** **]** **4.a, 4.b** <u>References:</u> [1] "Spent Nuclear Fuel Effective Thermal Conductivity Report," US DOE Report BBA000000-01717-5705-00010 REV 0, (July 11, 1996). [2] Hagrman, Reymann and Mason, "MATPRO-Version 11 (Revision 2) A Handbook of Materials Properties for Use in the Analysis of Light Water Reactor Fuel Rod Behavior," NUREG/CR-0497, Tree 1280, Rev. 2, EG&G Idaho, August 1981. [3] "Nuclear Systems Materials Handbook, Vol. 1, Design Data", ORNL TID 26666. [4] "Scoping Design Analyses for Optimized Shipping Casks Containing 1-, 2-, 3-, 5-, 7-, or 10-Year-Old PWR Spent Fuel", ORNL/CSD/TM-149 TTC-0316, (1983). [5] "Process Heat Transfer", D.Q. Kern.

RAI-07

Quality Assurance Program

In the topical report, Holtec did not discuss the quality assurance program which controlled this analysis. Holtec should confirm that this **[Proprietary Information Withheld per 10 CFR 2.390]** [4.a, 4.b] analysis is kept under a quality assurance program consistent with 10 CFR Part 50 Appendix B that this program contains adequate documentation for design control, document control, software configuration control and testing, and corrective actions, and that the analysis has been independently peer reviewed. Additionally, Holtec should confirm that the important references which the analysis method rely upon have been incorporated into Holtec's quality assurance program.

Regulatory Justification	SRP Section 15.0.2, Subsection III.3f				
Associated Section	3.3.6.1 Appendix B Quality Assurance Program				
Level of Concern	3	Level of Impact	3	Level of Effort	2
Overall Significance	Low				
Holtec Response	The analysis developed for this topical report was developed, reviewed and approved under the Holtec Quality Assurance (QA) Program. The Holtec QA Assurance Program addresses the 10 CFR 50, Appendix B requirements and provides for appropriate design control, document control, software configuration control and testing, and corrective actions. The topical report and the supporting analysis are maintained under the Holtec QA Program. When the methodology is approved and then is applied to a plant specific spent fuel pool, the site specific calculations will be performed in accordance with the site's Quality Assurance Program.				

RAI-08

Comparison to Office of Research (RES) Data

[

[PROPRIETARY INFORMATION WITHHELD PER 10 CFR 2.390]

] [4.a, 4.b] Please provide a plot similar to that given in Figure 7.3 with these comparisons

Regulatory Justification	SRP Section 15.0.2, Subsection III.3d				
Associated Section	3.3.3.2 Validation of the Evaluation Model				
Level of Concern	3	Level of Impact	5	Level of Effort	3
Overall Significance	Low				
Holtec Response	Figure 7.3 in the TR has been expanded to show data up to 6 months for BWR fuel assemblies. The revised figure compares data from the method proposed in the TR to data from calculations done by the Office of Research (RES) starting from 6 months of cooling time. The conclusions made in the TR still remain applicable that the proposed method shows conservative results under all configurations for BWR fuel assemblies **[Proprietary Information Withheld per 10 CFR 2.390.]** [4.a, 4.b] A similar figure has been added to the TR for PWR fuel assemblies.				

Response to RAI-08

Revised Figure 7.3

4.a, 4.b

[PROPRIETARY INFORMATION WITHHELD PER 10 CFR 2.390]

RAI-09

Variation in Heat Capacity **[** **[PROPRIETARY INFORMATION WITHHELD PER 10 CFR 2.390]** **]** **4.a, 4.b**					
Regulatory Justification	SRP Section 15.0.2, Subsection III.3b				
Associated Section	3.3.1.4 Level of Detail in the Model				
Level of Concern	3	Level of Impact	3	Level of Effort	4
Overall Significance	Low				
Holtec Response	Heat capacity of fuel assemblies is an input to the calculations. **[** **[PROPRIETARY INFORMATION WITHHELD PER 10 CFR 2.390]** **]** **4.a, 4.b**				

Enclosure 3

Affidavit for Withholding

(5 Pages Attached)

U.S. Nuclear Regulatory Commission
ATTN: Document Control Clerk
Non-Proprietary Enclosure 3

AFFIDAVIT PURSUANT TO 10 CFR 2.390

I, Andrea L. Sterdis, being duly sworn, depose and state as follows:

1) I have reviewed the information provided in the RAI responses provided in Enclosure 1 which is sought to be withheld, and am authorized to apply for its withholding.

2) The information sought to be withheld is in Enclosure 1 to the May 27, 2021 letter to NRC providing "Responses to Request for Additional Information - Holtec Spent Fuel Pool Heat Up Calculation Methodology Topical Report." The Enclosure 1 responses contain information that is proprietary to Holtec International.

3) In making this application for withholding of proprietary information of which it is the owner, Holtec International relies upon the exemption from disclosure set forth in the Freedom of Information Act ("FOIA"), 5 USC Sec. 552(b)(4) and the Trade Secrets Act, 18 USC Sec. 1905, and NRC regulations 10 CFR Part 9.17(a)(4), 2.390(a)(4), and 2.390(b)(1) for "trade secrets and commercial or financial information obtained from a person and privileged or confidential" (Exemption 4). The material for which exemption from disclosure is here sought is all "confidential commercial information", and some portions also qualify under the narrower definition of "trade secret", within the meanings assigned to those terms for purposes of FOIA Exemption 4 in, respectively, Critical Mass Energy Project v. Nuclear Regulatory Commission, 975F2d871 (DC Cir. 1992), and Public Citizen Health Research Group v. FDA, 704F2d1280 (DC Cir. 1983).

AFFIDAVIT PURSUANT TO 10 CFR 2.390

4) Some examples of categories of information which fit into the definition of proprietary information are:

   a. Information that discloses a process, method, or apparatus, including supporting data and analyses, where prevention of its use by Holtec's competitors without license from Holtec International constitutes a competitive economic advantage over other companies;

   b. Information which, if used by a competitor, would reduce his expenditure of resources or improve his competitive position in the design, manufacture, shipment, installation, assurance of quality, or licensing of a similar product.

   c. Information which reveals cost or price information, production, capacities, budget levels, or commercial strategies of Holtec International, its customers or its suppliers;

   d. Information which reveals aspects of past, present, or future Holtec International customer-funded development plans and programs of potential commercial value to Holtec International;

   e. Information which discloses patentable subject matter for which it may be desirable to obtain patent protection.

   The information sought to be withheld is considered to be proprietary for the reasons set forth in paragraphs 4.a and 4.b, and 4.c above.

5) The information sought to be withheld is being submitted to the NRC in confidence. The information (including that compiled from many sources) is of a sort customarily held in confidence by Holtec International, and is in fact so held. The information sought to be withheld has, to the best of my knowledge and belief, consistently been held in confidence by Holtec International. No public disclosure has been made, and it is not available in public sources. All disclosures to third parties, including any required transmittals to the NRC, have been made, or must be made, pursuant to regulatory provisions or proprietary agreements which provide for maintenance of the information in confidence. Its

AFFIDAVIT PURSUANT TO 10 CFR 2.390

initial designation as proprietary information, and the subsequent steps taken to prevent its unauthorized disclosure, are as set forth in paragraphs (6) and (7) following.

6) Initial approval of proprietary treatment of a document is made by the manager of the originating component, the person most likely to be acquainted with the value and sensitivity of the information in relation to industry knowledge. Access to such documents within Holtec International is limited on a "need to know" basis.

7) The procedure for approval of external release of such a document typically requires review by the staff manager, project manager, principal scientist or other equivalent authority, by the manager of the cognizant marketing function (or his designee), and by the Legal Operation, for technical content, competitive effect, and determination of the accuracy of the proprietary designation. Disclosures outside Holtec International are limited to regulatory bodies, customers, and potential customers, and their agents, suppliers, and licensees, and others with a legitimate need for the information, and then only in accordance with appropriate regulatory provisions or proprietary agreements.

8) The information classified as proprietary was developed and compiled by Holtec International at a significant cost to Holtec International. This information is classified as proprietary because it contains detailed descriptions of analytical approaches and methodologies not available elsewhere. This information would provide other parties, including competitors, with information from Holtec International's technical database and the results of evaluations performed by Holtec International. A substantial effort has been expended by Holtec International to develop this information. Release of this information would improve a competitor's position because it would enable Holtec's competitor to copy our technology and offer it for sale in competition with our company, causing us financial injury.

9) Public disclosure of the information sought to be withheld is likely to cause substantial harm to Holtec International's competitive position and foreclose or reduce the availability of profit-making opportunities. The information is part of

AFFIDAVIT PURSUANT TO 10 CFR 2.390

Holtec International's comprehensive decommissioning and spent fuel storage technology base, and its commercial value extends beyond the original development cost. The value of the technology base goes beyond the extensive physical database and analytical methodology, and includes development of the expertise to determine and apply the appropriate evaluation process.

The research, development, engineering, and analytical costs comprise a substantial investment of time and money by Holtec International.

The precise value of the expertise to devise an evaluation process and apply the correct analytical methodology is difficult to quantify, but it clearly is substantial.

Holtec International's competitive advantage will be lost if its competitors are able to use the results of the Holtec International experience to normalize or verify their own process or if they are able to claim an equivalent understanding by demonstrating that they can arrive at the same or similar conclusions.

The value of this information to Holtec International would be lost if the information were disclosed to the public. Making such information available to competitors without their having been required to undertake similar expenditure of resources would unfairly provide competitors with a windfall, and deprive Holtec International of the opportunity to exercise its competitive advantage to seek an adequate return on its large investment in developing these very valuable analytical tools.

U.S. Nuclear Regulatory Commission
ATTN: Document Control Clerk
Non-Proprietary Enclosure 3

AFFIDAVIT PURSUANT TO 10 CFR 2.390

STATE OF SOUTH CAROLINA)
) ss:
COUNTY OF RICHLAND)

Andrea L. Sterdis, being duly sworn, deposes and says:

That she has read the foregoing affidavit and the matters stated therein are true and correct to the best of her knowledge, information, and belief.

Executed at Blythewood, South Carolina, this 27 day of May 2021.

Andrea L. Sterdis
Holtec Decommissioning International
Holtec International
VP, Regulatory & Environmental Affairs

Subscribed and sworn before me this 27 day of May, 2021

Christina G. Shaffer
exp. date 11/5/28

CHRISTINA G. SHAFFER NOTARY PUBLIC SOUTH CAROLINA

Enclosure 4

Reference 2.1 (RAI Response RAI-02)

"Effective Thermal Conductivity and Edge Conductance

Model for a Spent-Fuel Assembly"

(20 Pages Attached)

EFFECTIVE THERMAL CONDUCTIVITY AND EDGE CONDUCTANCE MODEL FOR A SPENT-FUEL ASSEMBLY

HEAT TRANSFER AND FLUID FLOW

KEYWORDS: *heat transfer, spent fuel, effective thermal conductivity*

RANDALL D. MANTEUFEL *Southwest Research Institute*
Center for Nuclear Waste Regulatory Analyses, 6220 Culebra Road
San Antonio, Texas 78238-5166

NEIL E. TODREAS *Massachusetts Institute of Technology*
Department of Nuclear Engineering, 77 Massachusetts Avenue
Cambridge, Massachusetts 02139

Received December 7, 1992
Accepted for Publication July 21, 1993

An effective thermal conductivity (k_{eff}) and an edge thermal conductance (h_{edge}) model are developed for the interior and edge regions of a spent-fuel assembly residing in an enclosure. The model includes conductive and radiative modes of heat transfer. Predictions using the proposed k_{eff}/h_{edge} model are compared with five sets of experimental data for validation. The model is compared with predictions generated by the engine maintenance, assembly, and disassembly (E-MAD) and Wooton-Epstein correlations, which represent the state of the art in this field. The model is applied to a typical pressurized water reactor and a typical boiling water reactor spent-fuel assembly, and a set of both nonlinear and linear formulations of the model are derived. The proposed model is based on rigorous models of the governing heat transfer mechanisms and can be applied to a large range of assembly and enclosure types, enclosure temperatures, and assembly decay heat values. The proposed model is more accurate than comparable lumped correlations and is more amenable for simple, repetitive design applications than other detailed numerical models.

I. INTRODUCTION

In a typical transportation or storage cask, each spent-fuel assembly resides in a square enclosure that is backfilled with a nonoxidizing gas (usually helium or nitrogen).[1-4] For design purposes, it is desirable to have a simple yet accurate method to predict the maximum fuel rod temperature in a spent-fuel assembly in these casks. Regulations pertinent to spent-fuel shipping and storage require that the spent-fuel cladding be protected from degradation (10CFR71.43d for transportation casks[5] and 10CFR72.122h for storage casks[6]). The degradation of spent-fuel cladding has been investigated and found to be accelerated by prolonged exposure in an oxidizing environment at elevated temperatures.[7-9] Hence, the casks are typically backfilled with a nonoxidizing gas, and the maximum temperature is maintained below the design limit of ~380°C. Frequently, casks are designed to efficiently dissipate the decay heat of the spent fuel so that this design goal is achieved with relatively large margins of safety, especially for spent fuel with long cooling periods.

The U.S. Department of Energy (DOE) is sponsoring the development of a new fleet of spent-fuel shipping casks.[10,11] One goal of the new fleet is to improve safety, as well as increase shipping payload, for the large number of fuel shipments expected to occur in the 21st century. Designers are encouraged to develop innovative designs that are based on technically defensible engineering methods. Consistent with these goals, analysis methods have continually been reviewed and updated to improve accuracy.

From a recent survey of preliminary shipping cask design reports,[1-4] it was found that a substantial fraction of the total cask temperature drop (from maximum fuel temperature to ambient environment temperature, i.e., $\Delta T_c = T_m - T_\infty$) is predicted to occur over a single assembly (from maximum fuel temperature to enclosure wall temperature, i.e., $\Delta T_a = T_m - T_w$). The survey is summarized in Table I, where it is noted that the temperature drop for a single assembly ranges from 15 to 31% of the total temperature drop (i.e., $\Delta T_a/\Delta T_c$). This is considered a significant fraction of the total cask temperature drop.

In addition, the prediction of ΔT_a has relatively large uncertainties because the most frequently used method to calculate ΔT_a is the Wooton-Epstein correlation.[13] The Wooton-Epstein correlation was originally

TABLE I

A Summary of Parameters and Methods Currently Being Used to Predict the Temperature Drop Due to a Single Assembly (ΔT_a) for Current Design Spent-Fuel Shipping Casks*

Cask Contractor Cask	Cask Type	Payload PWR/BWR	Gas	Q[a] (W)	T_m[b] (°C)	ΔT_a[c] (°C)	ΔT_c[d] (°C)	$\frac{\Delta T_a}{\Delta T_c}$ (%)	Method
Babcock & Wilcox BR-100 (Ref. 1)	Rail	21/52	Helium Helium	576 837	185 234	50 64	160 210	31 31	WE[e] WE
General Atomic GA-4/GA-9 (Ref. 4)	Truck	4/9	N_2	552	187	43	160	27	k_{eff}[f]
Westinghouse Titan (Ref. 3)	Truck	3/7	Helium	580	217	27	192	15	E-MAD[g]
Nuclear Assurance NAC (Ref. 2)	Rail	26/52	Helium	506	242	41	217	20	WE

*Updated from Ref. 12.
[a]Q = total assembly decay heat.
[b]T_m = calculated maximum assembly temperature.
[c]ΔT_a = temperature drop associated with an assembly.
[d]ΔT_c = total temperature drop for cask.
[e]WE = Wooton-Epstein correlation.[13]
[f]k_{eff} = effective conductivity model.
[g]E-MAD = E-MAD correlation.[14]

developed 30 yr ago, assuming only nitrogen backfill (while helium is now predominantly being used), assuming turbulent natural convection (where recent experimental evidence suggests laminar natural convection), and for much higher assembly decay heats (8 compared with 0.5 kW). Hence, a study of heat transfer within a spent-fuel assembly was conducted and is reported herein.

Many investigations have been reported on modeling heat transfer in a spent-fuel assembly since the work of Wooton and Epstein.[15-21] However, these models were not used in the recent transportation cask preliminary design reports[1-4] (see Table I for the models used). In addition, a large amount of recent modeling work is available to designers.[22-24] An obvious question is the following: Why has the 30-yr-old Wooton-Epstein correlation continued to be used in light of more recent work? Also, what will be the unique contribution of a new method compared with approaches already available in the literature? The answer involves (a) the inherent uncertainties in the physical problem and (b) the analysis cost associated with a method. From the discussion of each of these issues, the motivation for the development of the proposed model is made apparent.

I.A. Uncertainties

A number of significant uncertainties are associated with heat transfer within a spent-fuel assembly: (a) fuel rod emissivity, (b) enclosing wall emissivity, (c) net assembly decay power, (d) axial decay peaking factor, and (e) backfill gas composition.[12] Specifically, the current state of knowledge suggests that each of these quantities have uncertainties ranging from at least 10 to as much as 25%. For example, the spent-fuel rod emissivity is expected to have a value between 0.6 and 1.0 with a probability of 95% (where the mean is 0.8 and one standard deviation is 0.1), which represents a 25% uncertainty about the typically assumed value of 0.8 (Ref. 25). The large range of emissivity values appears primarily to be the result of differences in the experimental results from five separate investigations using different states of oxidation (e.g., uniform oxide, nodular oxide, or oxide with crud). If radiative heat transfer is the dominant heat transfer mechanism (as it is for nitrogen backfill with $T > 200$°C), then the prediction of ΔT_a should be expected to have an ~25% uncertainty due to the uncertainty in the emissivity value. This is a significant uncertainty that would overwhelm most approximation errors introduced in the development of more exact theoretical models. It is presumed that the pragmatic cask designers recognize these inherent uncertainties and see the inappropriateness of performing more exact theoretical analyses than the knowledge of input parameters supports.

I.B. Simple Methods

Coupled with uncertainties in data, the task of performing analyses and developing designs strongly suggests using simple, conservative models coupled with

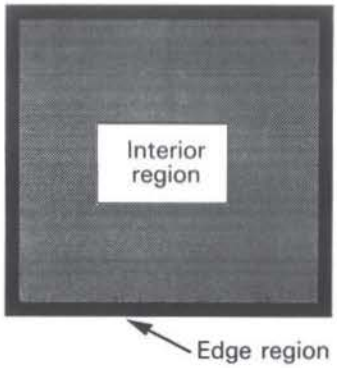

Fig. 2. Homogeneous idealization of an enclosed rod array that includes both an interior and an edge region.

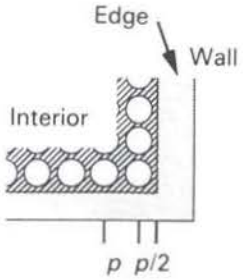

Fig. 3. Idealization of an enclosed assembly where the assembly is smaller than the enclosure and is assumed to reside in the center of the enclosure.

is neglected here, yet it will be discussed briefly in Sec. III.A. The combined conductive and radiative conductivity yields the total effective conductivity:

$$k_{eff} = k_{cond} + k_{rad} \ . \tag{1}$$

The conductive component is discussed in Sec. II.A.1, and the radiative component is discussed in Sec. II.A.2.

II.A.1. Stagnant-Gas Conduction

The effective conductivity of a composite medium consisting of infinitely long tubes residing in a medium has been considered in the literature.[29,30] The effective stagnant-gas conductive conductivity is frequently related to the backfill gas conductivity through a conduction factor:

$$k_{cond} = F_{cond} k_{gas} \ , \tag{2}$$

where

k_{cond} = effective conductivity assuming the backfill gas is stagnant

F_{cond} = conduction factor

k_{gas} = backfill gas conductivity.

The problem is to calculate F_{cond} as a function of tube array pattern (square or hexagonal), characteristic geometrical data (rod diameter, rod-to-rod pitch, cladding thickness), and conductivities (k_{gas}, k_{clad}, and k_{fuel}). A set of analytic formulas for the effective conductivity has been derived analytically.[30] A relatively simple analytic formula has been found to be accurate for pitch-to- diameter (p/d) ratios near typical nuclear fuel assembly values (but not for small p/d ratios such as found in consolidated applications where more accurate formula are required). For illustration purposes, the simple formula is presented here:

$$F_{cond} = \frac{1 - f v_1}{1 + f v_1} \ , \tag{3}$$

where

f = volume fraction of the tubes (or rods)

v_1 = coefficient depending on the tube dimensions and conductivities.

For a square array of rods, the volume fraction is given by

$$f = \frac{\pi}{4(p/d)^2} \ , \tag{4}$$

which is approximately equal to 0.444 for $p/d = 1.33$.

Representative values for the conductivities are $k_{fuel} = 5$ W/(m·°C), $k_{clad} = 15$ W/(m·°C), and $k_{gas} =$ [0.2 W/(m·°C) for helium and 0.04 W/(m·°C) for nitrogen]. In practice, a gap exists between the fuel and the clad, and a thermal resistance to heat transfer is typically associated with this gap (i.e., gap thermal conductance). The value of the gap conductance is considered to be uncertain; hence, the conductivity of the fuel is frequently neglected ($k_{fuel} = 0.0$) in the calculation of F_{cond}. This underestimates the effective conductivity of the medium and leads to a higher estimate of the maximum temperature. The effect of this approximation has been compared to other approximations (i.e., assume the fuel has a conductivity equal to the gas, or assume negligible thermal resistance across the gap), and the differences were found to be insignificant.

The formula for the coefficient, assuming $k_{fuel} = 0$, is

$$v_1 = \frac{\delta_{gas\text{-}clad} + \left(\frac{r_i}{r_o}\right)^2}{1 + \delta_{gas\text{-}clad}\left(\frac{r_i}{r_o}\right)^2} \ , \tag{5}$$

where

$\delta_{gas\text{-}clad} = (k_{gas} - k_{clad})/(k_{gas} + k_{clad})$

r_i = inner radius of the clad wall

r_o = outer radius of the clad wall.

large factors of safety. This appears the most rational path that has been chosen by the designers surveyed in Table I. It is interesting to note that the highest maximum temperature reported in Table I is 242°C, which is significantly below the design goal of 380°C. This represents a significant factor of safety. Although computer programs are available to more accurately predict ΔT_a (assuming the input parameters are known with precision), there is currently no need to design close to the design limit, which would justify incurring the costs associated with acquiring, porting, learning, and running a complex code. In the future, the maximum temperature in actual cask loadings due to larger payloads or less-aged spent fuel may approach 380°C, and it may then be expected that cask designers would aggressively pursue more accurate thermal analysis methods.

In review, an objective of this work is to improve the state of the art in predicting the maximum temperature in a single spent-fuel assembly because of its importance to the overall ΔT for a cask. The calculation method currently preferred by cask designers was developed for a range of applications different than current conditions (especially higher decay power levels and predominantly helium backfill). In addition, although newer methods have been developed and published in the literature, they have not been adopted by cask designers. This is thought to be due to the increased complexity associated with the newer methods (1000+ line computer codes compared with a single algebraic equation) and the fact that these approaches are not supported by precise knowledge of many input parameters. Hence, this work was motivated to develop a new, theoretically based method for design use that is sufficiently accurate yet acceptably simple.

II. EFFECTIVE CONDUCTIVITY AND EDGE CONDUCTANCE MODEL

A typical pressurized water reactor (PWR) or boiling water reactor (BWR) fuel assembly has a small cross-sectional dimension (~15 to 21 cm square) in comparison with the axial length (~370 cm). Because of the small width-to-length ratio, the spent-fuel assemblies are typically modeled as two-dimensional cross sections. A two-dimensional cross section of an 8 × 8 array in a square enclosure is illustrated in Fig. 1. A typical BWR has an 8 × 8 array enclosed in a channel that is part of the fuel assembly, and a typical PWR has a 15 × 15 array but does not have a channel as part of the assembly.

For spent fuel, the spatial distribution of decay heat is generally described as being cross-sectionally uniform and nearly uniform along the long axis. No known sources specifically account for cross-sectionally varying decay heats; however, a number of computer codes appear to have this capability. In comparison, the axial variation in decay heat has been considered more important than the cross-section variation. Typically, a two-dimensional model is assumed (as shown in Fig. 1), a uniform decay heat (which is larger than the average decay heat) is assumed, and axial heat transfer is neglected. The maximum axial decay heat is assumed to be larger than the average decay heat by a factor of either $F_{peak} = 1.1$ (Refs. 1, 26, 27, and 28) or $F_{peak} = 1.2$ (Refs. 2 and 3).

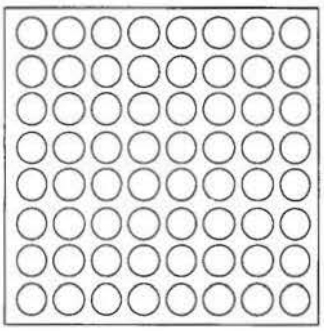

Fig. 1. Cross-sectional view of an enclosed 8 × 8 rod array.

A theoretical study of the conductive, convective, and radiative heat transfer mechanisms in an enclosed rod array has been completed,[12] and the pertinent results are summarized here, especially the application of the theory to develop an effective thermal conductivity (k_{eff}) and edge conductance (h_{edge}) model for a spent-fuel assembly. In this paper, four distinct formulations of the k_{eff}/h_{edge} model are discussed: the continuum form (Sec. II.A), the lumped form (Sec. II.B), the nonlinear algebraic form (Sec. IV.A), and the linear algebraic form (Sec. IV.B). The forms are progressively simpler, yet each form has additional assumptions or approximations in their derivation. The continuum form is the most general and is discussed next.

II.A. Continuum k_{eff}/h_{edge} Model

A spent-fuel assembly is modeled as having two primary regions: the interior region and an edge region, as shown in Fig. 2. The interior region is modeled as a homogeneous medium that has macroscopic thermal properties that reflect the net effects of the detailed thermal phenomena. An effective thermal conductivity model is developed for the interior region that accounts for both conductive and radiative heat transfer. An edge conductance model is developed for the edge region that is also based on models of both conductive and radiative heat transfer. The edge region extends from the enclosure wall to one-half the pitch from the outer row of rods, as illustrated in Fig. 3.

Two modes of heat transfer are considered within the interior of an assembly: stagnant-gas conduction and thermal radiation. From experimental evidence reported in the literature, heat transfer due to natural convection can be neglected in the storage and transport of spent fuel for the vast majority of cases of interest. For notational convenience, natural convection

The ratio of radii can be related to the outer fuel rod diameter and the cladding thickness:

$$\frac{r_i}{r_o} = 1 - 2\frac{t}{d} , \tag{6}$$

where

t = cladding thickness

d = rod outer diameter.

Representative values for PWR and BWR assemblies are $d = 10.7$ mm for PWRs and 12.2 mm for BWRs, and $t = 0.615$ mm for PWRs and 0.813 mm for BWRs (Refs. 31 and 32). Substitution of these values into Eqs. (6), (5), and (3) yields

$$F_{cond} = \begin{cases} 2.11 & \text{PWR with helium} \\ 2.48 & \text{PWR with } N_2 \\ 2.16 & \text{BWR with helium} \\ 2.49 & \text{BWR with } N_2 \end{cases} \tag{7}$$

The difference between the values of F_{cond} due to either the PWR or BWR is considered negligible in comparison to the difference due to either helium or nitrogen backfill. Hence, the distinction between PWR and BWR geometries is frequently neglected, and F_{cond} is taken simply as a function of the backfill gas (assuming a square array pattern, $p/d = 1.33$, representative cladding thicknesses, representative rod diameters, and representative values of the gas and cladding conductivities):

$$F_{cond} = \begin{cases} 2.1 & \text{with helium} \\ 2.4 & \text{with } N_2 \end{cases} . \tag{8}$$

These simple results are used in Sec. IV to analyze a typical PWR and a typical BWR assembly. More accurate estimates of F_{cond} are used in the comparison of the model predictions with experimental data in Sec. III.

II.A.2. Thermal Radiation

The radiative conductivity model for a square array is derived by considering radiative heat transfer in the one-dimensional symmetry section shown in Fig. 4. The radiative transfer across the surface (q''_{rad}) is established as a function of the discrete rod temperatures, rod emissivity, and geometric information (e.g., d and p). Each rod is assumed to be isothermal, which is an approximation that can be justified for spent-fuel rods.[12] The radiative transfer between rod surfaces is related to the radiative absorption factors between columns of rods (because of the symmetry surfaces, each rod in Fig. 4 represents an infinite column of rods). The net radiative heat flux through the surface is

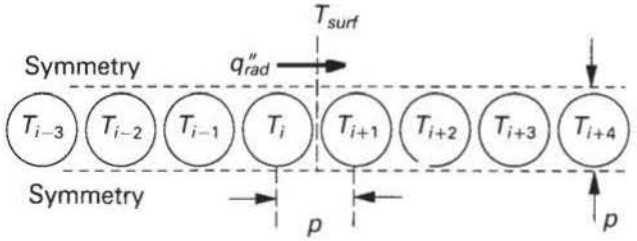

Fig. 4. One-dimensional symmetry section used in the derivation of the radiative conductivity in a square array.

$$q''_{rad} = \ldots + q''_{(i-2)-(i+1)} + q''_{(i-1)-(i+1)} + q''_{(i-1)-(i+2)} + q''_{i-(i+1)} + q''_{i-(i+2)} + q''_{i-(i+3)} + \ldots , \tag{9}$$

where

q''_{rad} = radiative flux across the imaginary surface

q''_{i-j} = radiative flux from column i to column j.

The radiative flux between columns of rods is given by

$$q''_{i-j} = \frac{\epsilon_r \pi d G_{i-j} \sigma}{p} (T_i^4 - T_j^4) , \tag{10}$$

where

ϵ_r = rod emissivity

G_{i-j} = column-to-column radiative absorption factor

T_i = temperature of rod i.

The column-to-column absorption factors are similar to Hottel's gray-body view factors (also called Hottel's script-F), where $\epsilon_r G_{i-j} = F_{i-j}$. The calculation of the G_{i-j} terms is accomplished by a Monte Carlo ray-tracing algorithm to calculate view factors and a matrix inversion algorithm to calculate absorption factors.[12]

The radiative conductivity is related to the total radiative heat flux through a discrete form of the Fourier's law (which in effect defines k_{rad} for this problem):

$$q''_{rad} = -k_{rad} \frac{\Delta T}{\Delta x} . \tag{11}$$

The temperatures for each rod are approximated as varying linearly from the imaginary surface between columns i and $i + 1$:

$$T_{i+n} \cong T_{surf} - \left(\frac{2n-1}{2}\right) p \frac{q''_{rad}}{k_{rad}} , \tag{12}$$

where n assumes any integer value (e.g., -2, -1, 0, 1, 2). The fourth power of temperature [as expressed in Eq. (10)] can be approximated using Eq. (12) [where $(a-b)^4 = a^4 - 4ba^3 + 6a^2b^2 - 4ab^3 + b^4$, and if $b \ll a$, then $(a-b)^4 \simeq a^4 - 4ba^3$]:

$$T_{i+n}^4 \cong T_{surf}^4 - \left(\frac{2n-1}{2}\right) p \frac{q''_{rad}}{k_{rad}} 4T_{surf}^3 \ . \quad (13)$$

Equation (13) can be substituted into Eqs. (9) and (10), and through a series of algebraic manipulations, the radiative conductivity can be expressed as

$$k_{rad} = C_{rad}\sigma\pi d4T^3 \ , \quad (14)$$

where C_{rad} is the radiative coefficient. In Eq. (14), the "surf" subscript on temperature has been dropped since the radiative conductivity is based on the local temperature. The radiative coefficient is related to the column-to-column absorption factors [which are introduced in Eq. (10)] as

$$C_{rad} = \epsilon_r [G_{i-(i+1)} + 2^2 G_{i-(i+2)} + \ldots + n^2 G_{i-(i+n)}] \ . \quad (15)$$

The value C_{rad} can be calculated numerically or approximated analytically. The computation of C_{rad} is not the primary focus of this paper; hence, the value of interest is simply stated. For a square array of rods, with $p/d = 1.33$ and rod emissivity $\epsilon_r = 0.8$, and the radiative coefficient has been calculated to be $C_{rad} = 0.4$ (Ref. 12). For the calculations presented in Sec. III, C_{rad} was evaluated for different conditions.

II.A.3. Edge Models

Similar to the interior model, stagnant-gas conduction and thermal radiation models are developed for the edge region. The edge is defined as the region from one-half the pitch from the outer row of rods to the enclosure wall, as illustrated in Fig. 3. A total edge conductance can be developed as consisting of a conductive and a radiative component:

$$h_{edge} = h_{cond} + h_{rad} \ , \quad (16)$$

where

h_{edge} = edge conductance (or edge heat transfer coefficient)

h_{cond} = wall conductive heat transfer coefficient

h_{rad} = wall radiative heat transfer coefficient.

The development of h_{cond} is straightforward algebraic manipulation following the same principles as outlined for the interior region (Sec. II.A.2) (Ref. 12), and the result is only summarized here:

$$h_{cond} = \frac{F_{cond,w} k_{gas}}{(1 - f/2)w} \ , \quad (17)$$

where

$F_{cond,w}$ = conduction factor for the wall

f = edge-to-interior heat transfer ratio

w = distance from the center of the outer ring of rods to the wall.

The wall conduction factor is defined as

$$F_{cond,w} = \begin{cases} F_{cond} \ , & w/p \le \frac{1}{2} \\ \dfrac{F_{cond}\, w/p}{\frac{1}{2} + F_{cond}(w/p - \frac{1}{2})} \ , & w/p > \frac{1}{2} \ . \end{cases} \quad (18)$$

The wall radiative coefficient is developed with the aid of Fig. 5, where the column-to-wall radiative absorption factors are introduced. In summary, the radiative coefficient was derived as:

$$h_{rad} = \frac{C_{rad,w,2}\sigma\pi d4(T_{f,w})^3}{(1 - f/2)p} \ , \quad (19)$$

where

$C_{rad,w,2}$ = second-wall radiative coefficient

σ = Stefan-Boltzmann constant [$= 5.67 \times 10^{-8}$ W/(m$^2 \cdot$K^4)]

$T_{f,w}$ = wall "film" temperature.

The wall film temperature is

$$T_{f,w} = \frac{T_e + T_w}{2} \ , \quad (20)$$

and the edge-to-interior heat transfer ratio is

$$f = \frac{F_{cond,w} k_{gas} p/w + C_{rad,w,1}\sigma\pi d4T^3}{F_{cond} k_{gas} + C_{rad}\sigma\pi d4T^3} \ , \quad (21)$$

where $C_{rad,w,1}$ is the second-wall radiative coefficient. The extrapolated temperature T_e is used in Eq. (20) and represents the temperature of an imaginary surface located at a distance one-half pitch from the center of the outer row of rods. The wall temperature T_w is the temperature of the enclosure. These temperatures are also discussed in Sec. II.B.

The wall radiative coefficients are based on the column-to-wall radiative absorption factors:

$$C_{rad,w,1} = \epsilon_r [G_{1-w} + 3G_{2-w} + \ldots + (2n-1)G_{n-w}] \quad (22)$$

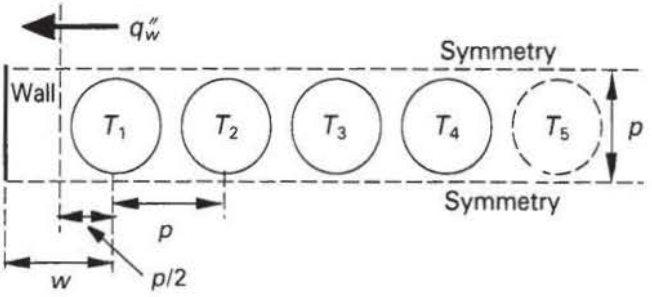

Fig. 5. One-dimensional symmetry section used in the derivation of the wall radiative heat transfer coefficient for a square array.

and

$$C_{rad,w,2} = \epsilon_r [G_{1-w} + G_{2-w} + \ldots + G_{n-w}] \ . \quad (23)$$

The column-to-wall radiative absorption factors are calculated by using the same techniques as the column-to-column absorption factors (described in Sec. II.A.2). For a square array of rods with $p/d = 1.33$, $\epsilon_r = 0.8$, and $\epsilon_w = 0.2$, the coefficients were calculated to be $C_{rad,w,1} = 0.105$ and $C_{rad,w,2} = 0.085$. The coefficients are calculated for different conditions in Sec. III.

II.B. Lumped k_{eff}/h_{edge} Model

A more convenient form of the k_{eff}/h_{edge} model can be developed from the continuum form, in order to quickly estimate the maximum fuel temperature in an array. The heat diffusion equation is solved for the interior region of the assembly in order to develop the lumped formulation of the k_{eff}/h_{edge} model. Three distinct temperatures are considered in the lumped k_{eff}/h_{edge} model: the maximum temperature T_m, the extrapolated temperature T_e, and the wall temperature T_w (see Fig. 6). The locations of T_m and T_w are considered logical, while T_e is located at an imaginary surface that is the extrapolated boundary of the interior region. The nonlinear conduction equation is solved for the interior region assuming the heat generation is spatially uniform and the extrapolated wall temperature is circumferentially uniform. The temperature dependence of the radiative component of the effective conductivity can be solved (without additional approximations) using Kirchoff's transformation.

In general, the nonlinear heat conduction equation can be solved for square, hexagonal, or circular cross-sectional geometries, as shown in Fig. 7. These geometries are of interest because the square cross section is a common configuration for PWR and BWR assemblies, the hexagonal cross section is common for liquid-metal reactor assemblies and light water reactor assemblies from Eastern European countries, and the circular cross section may be applicable to consolidated assemblies stored in a circular canister.

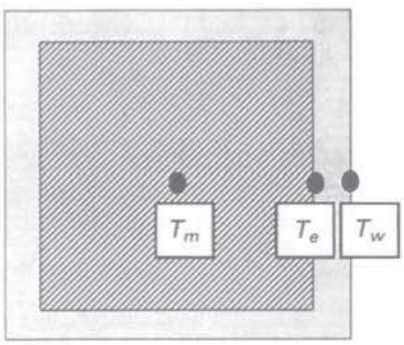

Fig. 6. Locations of the maximum, extrapolated, and wall temperatures.

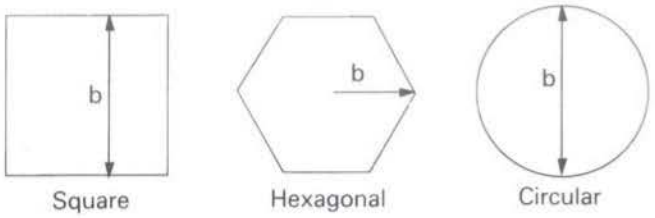

Fig. 7. Square, hexagonal, and circular cross-sectional geometries for which a conduction shape factor can be calculated [see Eq. (25)].

The solution of the heat diffusion equation can be expressed in a single equation valid for all three of the geometries:

$$\frac{QF_{peak}}{SL_a} = k_{eff}(T_m - T_e) \ , \quad (24)$$

where

Q = total assembly decay power

F_{peak} = axial decay heat peaking factor

L_a = thermally active axial length of the assembly

S = geometry-dependent conduction shape factor.

The only term that depends on the geometry is the shape factor. For each geometry, the shape factor has been calculated[12]:

$$S = \begin{cases} 13.5738 & \text{square} \\ 12.8365 & \text{hexagonal} \\ 4.0\pi & \text{circular} \end{cases} . \quad (25)$$

Hence, the lumped k_{eff}/h_{edge} model can be applied to the most probable fuel assembly geometries.

The lumped k_{eff}/h_{edge} model can be expressed in two coupled algebraic equations where the first equation applies to the assembly interior:

$$\frac{QF_{peak}}{SL_a} = F_{cond} k_{gas}(T_m - T_e) + C_{rad}\sigma\pi d(T_m^4 - T_e^4) \quad (26)$$

and the second equation to the edge region within the enclosing wall:

$$\frac{QF_{peak}}{L_a L_c} = \frac{F_{cond,w} k_{gas}}{(1 - f/2)w}(T_e - T_w) + \frac{C_{rad,w,2}\sigma\pi d}{(1 - f/2)p}(T_e^4 - T_w^4) \ . \quad (27)$$

Each of the variables in Eqs. (26) and (27) was previously introduced in Sec. II.A. As presented, Eqs. (26) and (27) represent the lumped formulation of the k_{eff}/h_{edge} model.

III. EXPERIMENTAL VALIDATION

The lumped k_{eff}/h_{edge} model predictions have been compared with five sets of experimental data in order to validate the proposed method. The five sets of data are from the engineering, maintenance, and disassembly (E-MAD) tests,[14] single assembly heat transfer tests[26] (SAHTT), Ridihalgh, Eggers, and Associates (REA) tests,[33] Sandia National Laboratories liquid-metal fast breeder reactor (SNL-LMFBR) tests,[34] and Massachusetts Institute of Technology (MIT) 8 × 8 tests.[35] The comparison of model predictions with experimental data is discussed for each test.

III.A. The E-MAD tests

A series of experimental tests were conducted at the E-MAD facility at the Nevada Test Site.[14,36,37] Extensive temperature measurements were recorded for two standard 15 × 15 Westinghouse PWR spent-fuel assemblies. The assemblies had average decay thermal powers of ~1300 and 750 W, respectively. Each assembly was placed within a cylindrical enclosure (called a canister) for a 2- to 3-yr testing period during which backfill gas and canister temperatures were controlled. The backfill gases were intermittently changed to include helium, air (which is thermally equivalent to nitrogen), and vacuum.

The vacuum pressure was reported to be 13.3 kPa (~100 mm Hg) of absolute pressure, which is considered to be a "weak" vacuum and insufficient to eliminate conduction in the backfill gas. The low pressure in the vacuum tests was, however, very effective at reducing the importance of natural convection (because the Rayleigh number scales as the total gas pressure squared for an ideal gas). In addition, it was estimated that the helium tests were conducted with ~80% helium and 20% air due to the relatively weak vacuum used to purge the air while changing to helium backfill.[12]

The lumped k_{eff}/h_{edge} model [Eqs. (26) and (27)] was used to predict the maximum fuel temperature (expressed as $\Delta T_a = T_m - T_w$). The input parameters (i.e., canister temperature, assembly decay heat, backfill gas, fuel rod emissivity, and canister emissivity) were either obtained directly from the E-MAD report[14] or from other sources that analyzed the test data.[27,28]

The test data and the model predictions are compared in Fig. 8 for tests conducted with helium backfill and in Fig. 9 for tests conducted with either vacuum or air backfill. As it can be noted, the model slightly overpredicts the maximum temperature, due in part to the conservative approximations introduced in the model, and conservative estimates of model parameters such as conduction factors and radiative coefficients.

The importance of natural convection can be seen in Fig. 9, where the air data yield lower values of ΔT than the vacuum data, especially at lower canister temperatures. The lower values of ΔT are assessed to be due

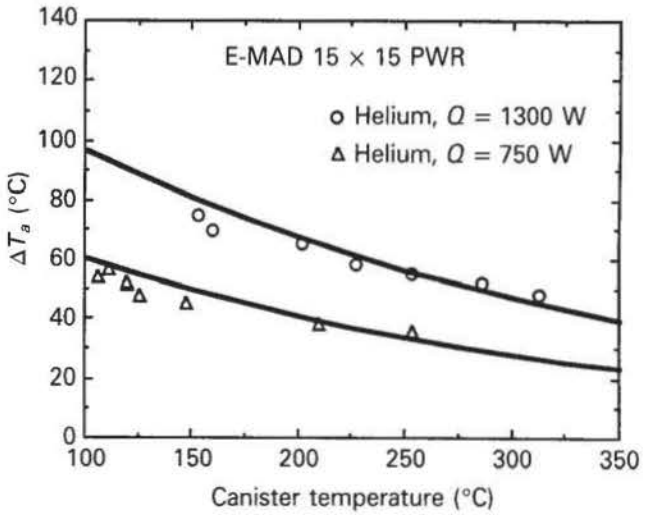

Fig. 8. Comparison of lumped k_{eff}/h_{edge} model predictions (solid lines) with experimental data from E-MAD tests with helium (80% helium and 20% air) backfill.

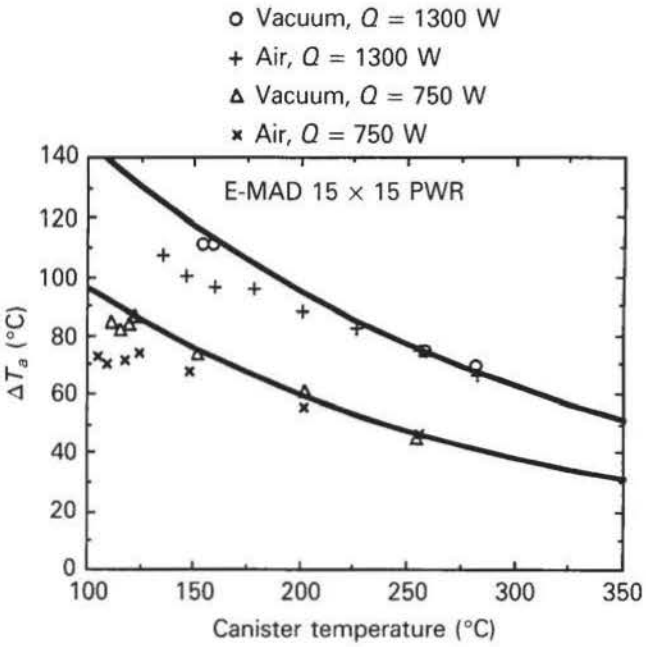

Fig. 9. Comparison of lumped k_{eff}/h_{edge} model predictions neglecting natural convection (solid lines) with experimental data from E-MAD tests with vacuum (~600 mm Hg) and air backfill.

to convection heat transfer. Based on a review[12] of experimental work,[20,38,39] a model was formulated to account for natural convection by increasing the effective conductive conductivity:

$$k_{cond} = \begin{cases} F_{cond} k_{gas} , & \mathrm{Ra} \le \mathrm{Ra}_{crit} \\ F_{cond} k_{gas} \left(\dfrac{\mathrm{Ra}}{\mathrm{Ra}_{crit}} \right)^{1/4} , & \mathrm{Ra} > \mathrm{Ra}_{crit} , \end{cases} \quad (28)$$

where

Ra = Rayleigh number (not defined here, see Ref. 12)

Ra_{crit} = critical Rayleigh number.

Below Ra_{crit}, the flow of the gas has a negligible effect on the value of T_m, so that the gas can be modeled as being stagnant. Above Ra_{crit}, buoyancy-driven gas flows are sufficiently strong to affect the value of T_m. Experimental work has been performed to estimate the critical Rayleigh number for a vertical, enclosed heated rod array.[20] Based on the previous work, Ra_{crit} was estimated for the E-MAD geometry and thermal conditions and has been included in the theoretical predictions. It was found, however, that good agreement could be achieved by using a Ra_{crit} one decade larger than predicted by the correlation in Ref. 20, as shown in Fig. 10. Based on this value of Ra_{crit}, it was determined that the Rayleigh number did not exceed the critical value for helium backfill and exceeded the critical value for air by only one decade at T_w = 100°C.

As noted in Fig. 8, the difference between the air and vacuum data is distinguishable only at low canister temperatures. This is due primarily to two trends: (a) the Rayleigh number scales as $Ra \sim 1/T^4$ for an ideal gas, and (b) the radiative conductivity scales as $k_{rad} \sim T^3$ [see Eq. (14)]. Hence, as the bulk temperature of the spent-fuel assembly increases, the Rayleigh number decreases, leading to a decrease in the importance of convective heat transfer. In contrast, as the bulk temperature increases, the importance of radiative heat transfer rapidly increases. The combined effect is that natural convection becomes less important at higher temperatures, which is the area of primary design interest (i.e., near 380°C).

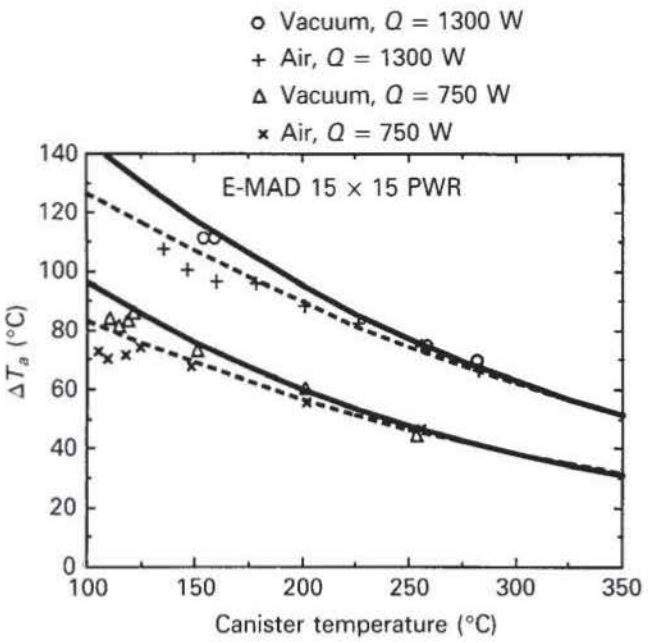

Fig. 10. Comparison of lumped k_{eff}/h_{edge} model predictions neglecting natural convection (solid lines) and including natural convection (dashed lines).

Correlations between ΔT_a and the assembly thermal power were developed in Ref. 14 for the E-MAD data and were used in the thermal analyses of spent-fuel storage[40,41] and shipping[3] casks. The correlations are for helium backfill:

$$\Delta T_a = Q(123.53 - 0.6325T_{can} + 0.001202T_{can}^2) \quad (29)$$

and for vacuum/air backfill:

$$\Delta T_a = Q[172.6 \times 10^{-(0.00179T_{can})}] , \quad (30)$$

where

Q = assembly thermal power (kW)

T_{can} = canister temperature (°C).

Equations (29) and (30) do not appear to have been developed by using models of conductive or radiative heat transfer. Finally, the vacuum/air equation reported in Ref. 41 is apparently in error (where the constant 0.00179 was reported to be 0.0000179) and has been corrected in Eq. (30).

The E-MAD correlations are compared with the lumped k_{eff}/h_{edge} predictions in Figs. 11 and 12. The E-MAD correlations (as well as the lumped k_{eff}/h_{edge} model predictions) are in good agreement with the experimental data. The only anomaly is that the E-MAD correlation for the helium backfill has a nonphysical increase in ΔT_a as T_{can} increases above 250°C. This is attributed to the quadratic nature of the correlation [see Eq. (29)]. Neither the experimental data nor the basic models of heat transfer (especially $k_{rad} \sim T^3$) support this trend in the E-MAD correlation.

The relative importance of conductive, convective, and radiative heat transfer were compared by using the lumped k_{eff}/h_{edge} model. In the array interior, the heat transfer due to conductive transport ranged from 40 to 60% with helium backfill and from 20 to 40% with air/vacuum backfill. The convective contribution ranged from a maximum of 20% at T_{can} = 100°C to 0% at T_{can} = 300°C. At the edge, the heat transfer due to conductive transport was less important than in the array interior primarily because of the large void region created by a square assembly residing in a circular enclosure. At the edge, the heat transfer due to radiative transport ranged from 55 to 85% with helium backfill and from 75 to 90% with air/vacuum backfill. Overall, the model predictions are considered to be in excellent agreement with the experimental data.

III.B. The SAHTT Tests

A series of SAHTT tests[26] were conducted by using an electrically simulated, full-scale 15 × 15 PWR

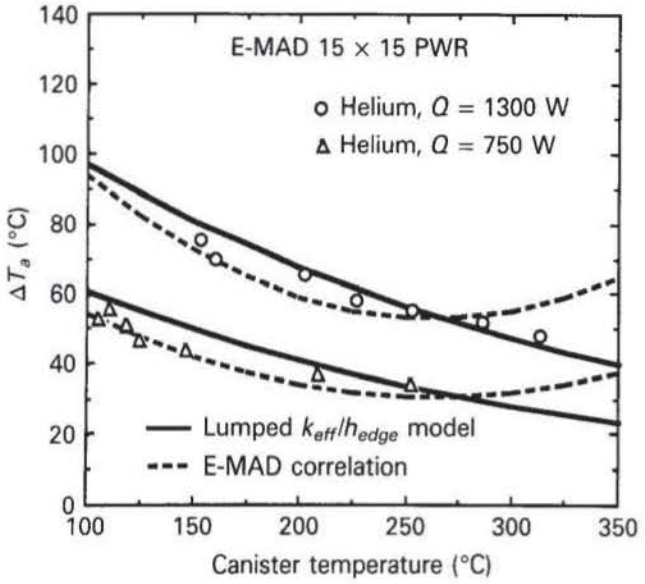

Fig. 11. Comparison of the lumped k_{eff}/h_{edge} model predictions (solid lines) with the E-MAD correlation (dashed lines) for helium backfill.

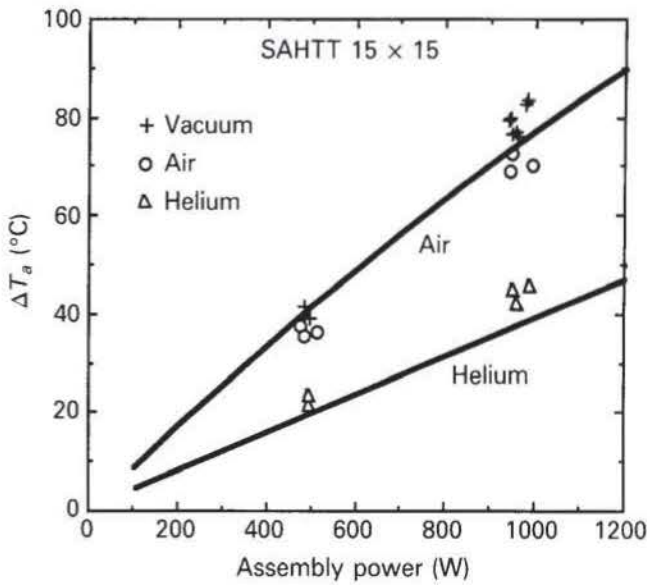

Fig. 13. Comparison of the lumped k_{eff}/h_{edge} model predictions (solid lines) with the experimental data from the SAHTT tests.

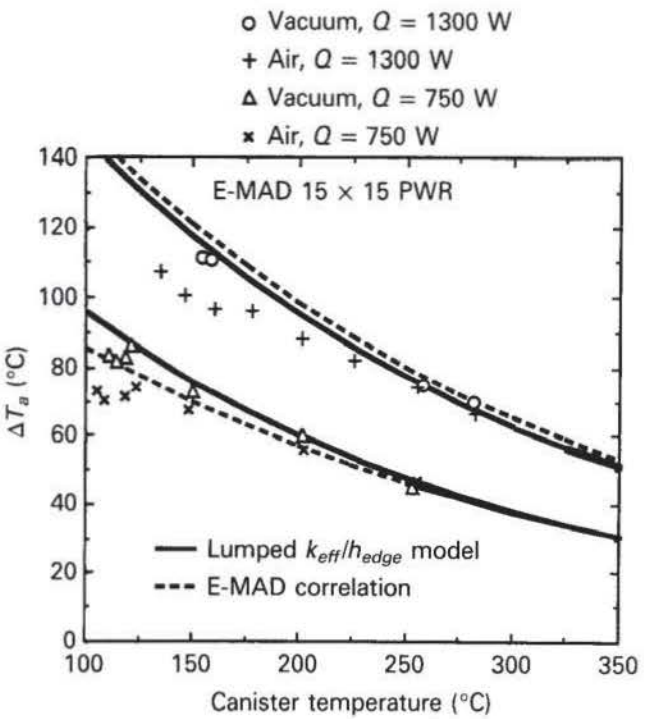

Fig. 12. Comparison of the lumped k_{eff}/h_{edge} model predictions (solid lines) with the E-MAD correlation (dashed lines) for vacuum and air backfill.

assembly. The assembly was enclosed in a fuel tube such as that found in storage and transportation casks. Experimental tests were conducted by using three different fill gases (helium, air, and vacuum), three axial orientations, and two power levels and with the canister temperature controlled using guard heaters to remain at 200°C. As in the E-MAD tests, the lowest reported vacuum pressure was 3.8 kPa (29 mm Hg) of absolute pressure so that natural convection was essentially eliminated in the vacuum tests; however, stagnant-gas conduction was not eliminated. The pertinent modeling parameters were either specified in the SAHTT report[26] or taken from other sources that analyzed the data.[27,28]

The lumped k_{eff}/h_{edge} model predictions (based on a constant tube temperature of 200°C) are compared with the experimental data in Fig. 13. The vacuum data show a slightly larger ΔT_a than the air data, indicating the effects of natural convection. However, the data have enough scatter that the effects of natural convection were assessed to be negligible in the enclosed tube bundle. Overall, there appears to be good agreement between the experimental data and the predictions. The k_{eff}/h_{edge} predictions in Fig. 13 were not "calibrated" to the experimental data (which would have improved the comparison) but are based on the best estimates of input parameters. An alternative explanation for the helium predictions being lower than the data is that the backfill gas was not 100% helium but contained a significant portion of air.

The relative importance of conductive and radiative heat transfer were compared based on the lumped k_{eff}/h_{edge} model. In the array interior, the percentage of heat transfer due to conduction ranged from 20 to 25% with air/vacuum backfill and from 55 to 60% with helium backfill. At the enclosure wall, the percentage of heat transfer due to conduction was ~45% with air/vacuum and ~75% with helium backfill. Overall, the model predictions are in agreement with the SAHTT experimental data.

III.C. The REA Tests

A series of tests[33] were conducted using an electrically simulated 61-cm (2-ft) section of an unconsolidated and a consolidated BWR. The consolidated tests were performed with two rod spacings ($p/d = 1.01$ and 1.02). Both the unconsolidated and consolidated arrays were emplaced in a square enclosure. The pertinent experimental details and parameters are taken from the REA report[33] and other sources that analyzed the data.[42] The unconsolidated tests were conducted with air and vacuum backfill, and the experimental data and lumped k_{eff}/h_{edge} model predictions are compared in Fig. 14. The lumped k_{eff}/h_{edge} model overpredicts the experimental ΔT_a, as did other model predictions reported in Ref. 42. One possible explanation for the difference is that axial conduction may be responsible for end heat losses (as suggested in Ref. 42). The previous predictions and those reported herein are considered comparable, so that no further investigation of the difference was pursued.

The lumped k_{eff}/h_{edge} model predicts that nearly 60% of the temperature drop occurred at the wall because of a relatively large wall-to-pitch ratio, $w/p = 1.45$, and a low wall emissivity, $\epsilon_w = 0.25$. Conduction accounts for ~20% of the total heat transfer in the interior of the assembly and ~25% at the wall. This indicates that radiative heat transfer was dominant in both the interior and edge regions (due primarily to a relatively high bulk temperature of 200°C and a low conductivity of the backfill).

The lumped k_{eff}/h_{edge} model predictions are compared with the consolidated data in Fig. 15 for both p/d values (1.01 and 1.02), both backfill gases (air and helium), and three power levels (100, 400, and 800 W). For the consolidated tests, the ΔT_a are considerably smaller than for the unconsolidated tests (~15 compared with ~50°C) for comparable power levels. This indicates that the effective conductivity for the consolidated tests was ~3.3 times higher than for the unconsolidated tests. For air backfill, the model predictions are assessed to slightly overestimate the experimental data, yet be in good agreement. For the helium backfill, the predictions underestimate the data, possibly because of axial heat transfer or air being present in the helium backfill.

III.D. The SNL-LMFBR Tests

Sandia National Laboratories conducted experiments using an electrically simulated 217-rod LMFBR fuel assembly.[34] The rods in the LMFBR assembly were arranged in a hexagonal array with $p/d = 1.24$ being maintained by axial wire wrappings around the rods. The rod array was enclosed within a hexagonal tube. Tests were conducted using helium backfill gas at power levels of 1000, 1250, and 1500 W.

The experimental data and the lumped k_{eff}/h_{edge} model predictions are compared in Fig. 16. The predictions consistently overpredict the experimental data yet appear to have the same trend of decreasing ΔT_a with

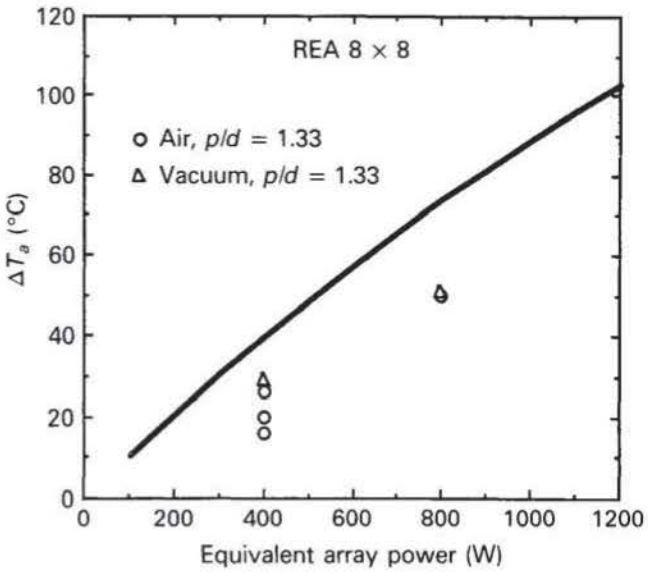

Fig. 14. Comparison of the lumped k_{eff}/h_{edge} model predictions (solid line) with the experimental data from the unconsolidated REA tests.

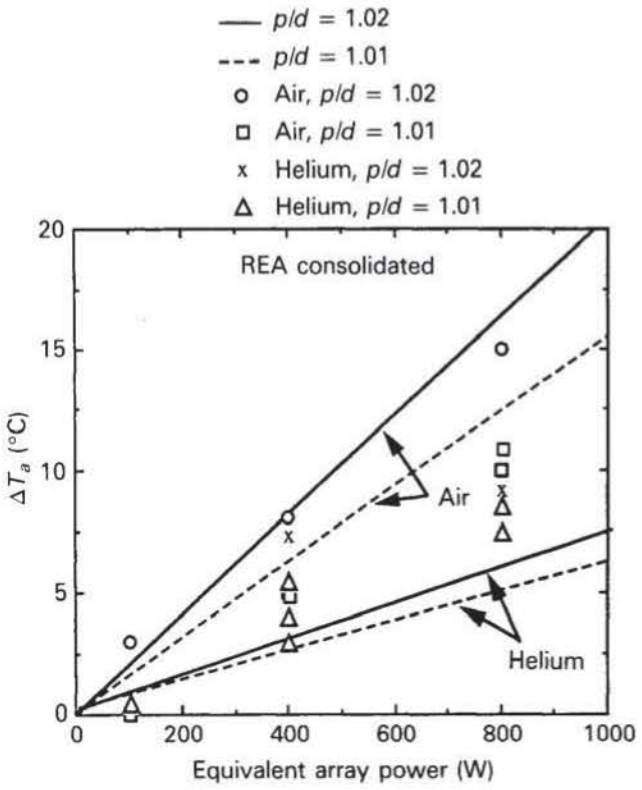

Fig. 15. Comparison of the lumped k_{eff}/h_{edge} model predictions (lines) with the experimental data from the consolidated REA tests.

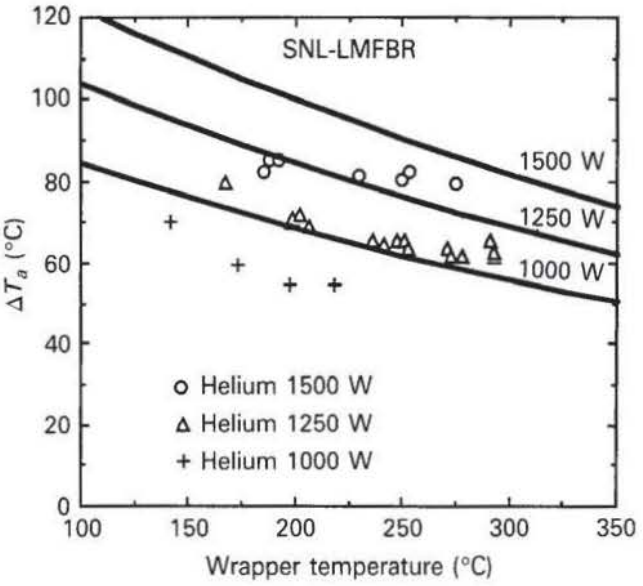

Fig. 16. Comparison of lumped k_{eff}/h_{edge} model predictions (solid lines) with experimental data from the SNL-LMFBR tests.

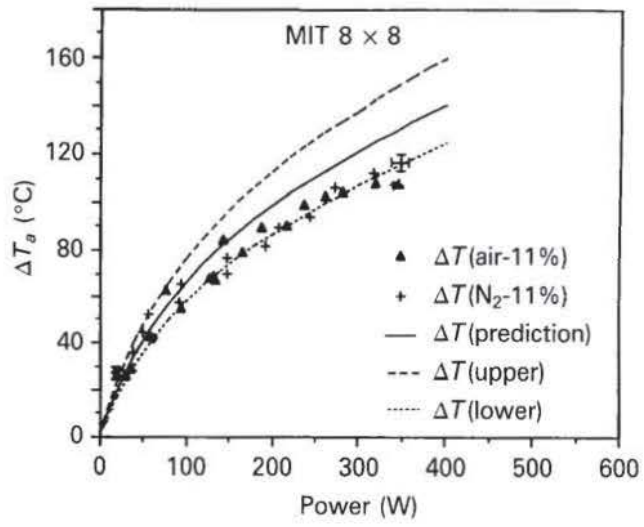

Fig. 17. Comparison of lumped k_{eff}/h_{edge} model predictions with experimental data from the MIT 8 × 8 tests with air and nitrogen backfills.[35]

increasing wrapper temperature. The overprediction appears to be primarily due to the neglect of the presence of the wire wrapping used to maintain the tight *p/d* in the LMFBR assembly. Overall, the data are properly oriented below the model predictions considering the enhanced conduction effect of the wire, so that these data are useful in validating the lumped k_{eff}/h_{edge} model.

III.E. The MIT 8 × 8 Tests

A series of electrically heated rod experiments[35] simulating a section (61 cm) of an 8 × 8 rod array was conducted at MIT. The rod array was enclosed in an aluminum box, and the backfill medium was intermittently changed to include air, nitrogen, and helium gas. The lumped k_{eff}/h_{edge} model predictions are compared with the experimental data in Figs. 17 and 18 for the air/nitrogen and helium tests, respectively. Best estimates of the experimental parameters are used to generate the solid lines (assuming 11% of the input heat was conducted axially and not accounted for; see Ref. 35), and the upper and lower estimates are based on the assessed uncertainties in the experimental parameters (shown as dash-dotted lines). The experimental data primarily fall within the bounds of predictions. Two general trends are that the model underpredicts the experimental data at low power values (especially for the helium backfill) and overpredicts the data at high power values. The source of these trends, however, is not apparent, but it is thought to be due to temperature measurement biases. Overall, the predictions are in good agreement with the MIT 8 × 8 experimental data.

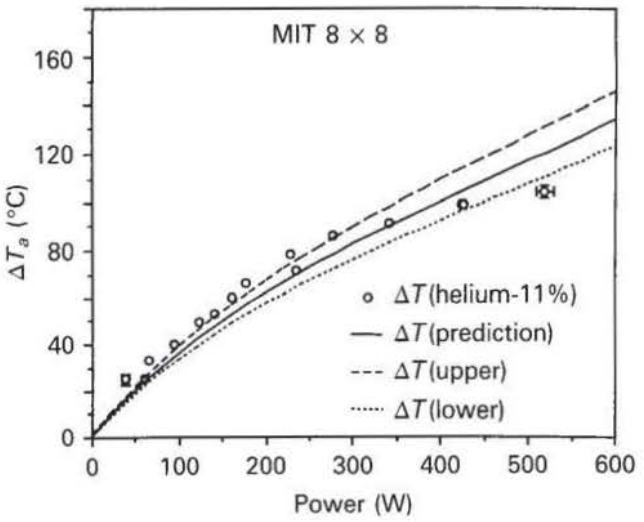

Fig. 18. Comparison of lumped k_{eff}/h_{edge} model predictions with experimental data from MIT 8 × 8 tests with helium backfill.[35]

IV. APPLICATION TO TYPICAL PWR AND BWR ASSEMBLIES

The lumped k_{eff}/h_{edge} model can be applied to a typical PWR and a typical BWR assembly in order to generate simplified equations that can readily be employed in the design of a cask. In particular, typical values are assumed for a PWR and a BWR assembly with either helium or nitrogen backfill. These typical values can be inserted into the lumped k_{eff}/h_{edge} model [Eqs. (26) and (27)] to generate two coupled nonlinear algebraic equations, which constitute the nonlinear algebraic form of the lumped k_{eff}/h_{edge} model (see Sec.

IV.A). For additional simplicity, the nonlinear equations can be linearized to generate the linear algebraic form of the lumped k_{eff}/h_{edge} model (see Sec. IV.B). Hence, two simplified forms (nonlinear and linear) of the lumped k_{eff}/h_{edge} model are presented in this section.

IV.A. Nonlinear Algebraic Form of the Lumped k_{eff}/h_{edge} Model

In practice, thermal analyses are performed by using characteristics for both a typical PWR and a typical BWR assembly.[1,4] For the current problem, Eqs. (26) and (27) can be applied to either of these assemblies, with either nitrogen or helium backfill, by using values from a comprehensive survey of spent-fuel characteristics.[31]

Typical values of input parameters for spent-fuel assemblies include for geometric parameters: $L_a = 3.66$ m, $p/d = 1.33$, $d \approx 0.0107$ m for a PWR and 0.0122 m for a BWR, $p = (p/d)d$, $L_c \approx 0.854$ m for a PWR and 0.556 m for a BWR, $w/p = 1.0$, $w = (w/p)p$. Typical values of input parameters for spent-fuel assemblies include four model parameters: $F_{peak} = 1.2$, $C_{rad} = 0.40$ (for a square array, $p/d = 1.33$ and $\epsilon_r = 0.8$), $F_{cond} \approx 2.1$ for helium and 2.4 for N_2, $k_{gas} \approx 0.2$ W/(m·°C) for helium and 0.04 W/(m·°C) for N_2, $C_{rad,w,2} = 0.085$, $F_{cond,w} = 1.355$ for helium and 1.412 for N_2 assuming $w/p = 1$, and $f = 0.45$ for helium and 0.33 for N_2. These parameter values have been inserted into Eqs. (26) and (27), leading to an interior equation:

$$Q = C_1(T_m - T_e) + C_2(T_m^4 - T_e^4) \qquad (31)$$

and an edge equation:

$$Q = C_3(T_e - T_w) + C_4(T_e^4 - T_w^4) \; . \qquad (32)$$

The coefficients (C_1, C_2, C_3, and C_4) in Eqs. (31) and (32) have been calculated and are presented in Table II. Typically, the total assembly thermal power Q and the average enclosure wall temperature T_w are specified as inputs, and the extrapolated wall temperature T_e and maximum temperature T_m are to be calculated. For illustration purposes, Eqs. (31) and (32) are solved by using the nonlinear, algebraic equation solver available in a commercially available mathematics program[43] for the typical PWR with either nitrogen (Fig. 19) or helium backfill (Fig. 20).

In Fig. 19, the predictions for a typical PWR with nitrogen backfill are plotted for three wall temperatures ($T_w = 100$, 200, and 300°C) and for a range of assembly decay powers ($100 < Q < 1500$ W). Note that increasing the wall temperature decreases ΔT_a because of the increased effectiveness of radiative heat transfer at higher temperatures. The curves for constant wall temperature are approximately linear at low assembly decay heats and are concave downward at the higher wall temperatures (this linearity is used in Sec. IV.B). For reference, the range of application for the current transportation cask designs (see Table I) is near $T_w = 200$°C and $Q \approx 500$ W, which yields $\Delta T_a = 40$°C from Fig. 19.

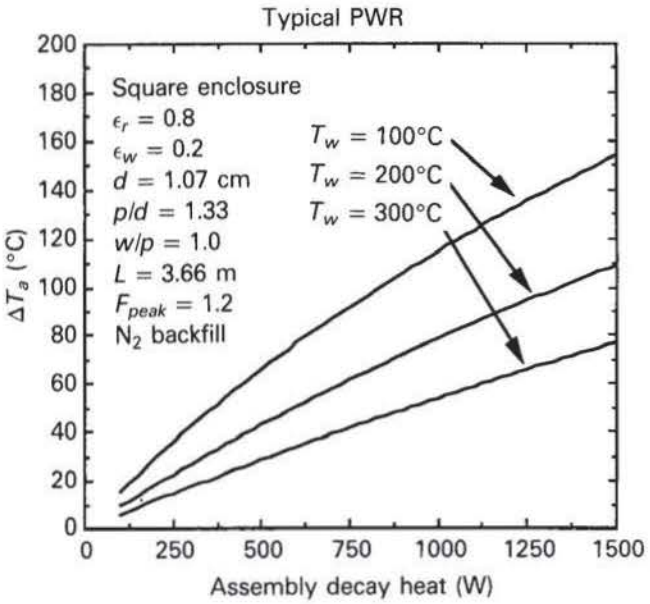

Fig. 19. Lumped k_{eff}/h_{edge} model predictions of ΔT_a for a typical PWR assembly with nitrogen backfill.

TABLE II

Coefficients in the Nonlinear Form of the Lumped k_{eff}/h_{edge} Model* for a Typical PWR and a Typical BWR Spent-Fuel Assembly in Either Helium or Nitrogen Backfill

	C_1 (W/K)	C_2 ($10^{-8} \times$ W/K^4)	C_3 (W/K)	C_4 ($10^{-8} \times$ W/K^4)
PWR with helium	17.38	3.16	64.0	3.83
PWR with N_2	3.97	3.16	12.38	3.55
BWR with helium	17.38	3.60	36.54	2.49
BWR with N_2	3.97	3.60	7.07	2.31

*Equations (31) and (32).

For higher fuel burnups and shorter cooling times, the assembly thermal power may exceed 1000 W; hence, the solutions are presented up to 1500 W.

Similarly, the results for helium backfill (compared with nitrogen backfill) are shown in Fig. 20. When comparing Figs. 19 and 20, it is noticeable that helium significantly reduces the ΔT_a (or equivalently the maximum temperature) because the thermal conductivity of helium is approximately five times larger than that of nitrogen.

The relative importance of conduction and radiation in both the interior region and the wall region of a typical PWR assembly are compared in Figs. 21 and 22. A general trend is that the radiation heat transfer becomes increasingly more important with increasing wall temperature. For the interior and edge regions of a typical PWR assembly, the general trends are as follows:

1. Conduction is more important when helium (rather than nitrogen) gas is used as the backfill.

2. The importance of conduction decreases as the wall temperature increases (likewise indicating an increasing importance of radiative heat transfer).

3. Conduction is more important at the edge of the array, compared with the interior of the array (based primarily on the input parameters: rod emissivity $\epsilon_r = 0.8$, enclosing wall emissivity $\epsilon_w = 0.2$, pitch-to-diameter ratio $p/d = 1.33$, wall-to-pitch ratio $w/p = 1.0$).

4. The importance of conduction is not strongly influenced by the assembly decay heat.

5. Conduction accounts for 10 to 30% of the total heat transfer in the interior and 30 to 55% at the edge of an enclosed PWR assembly with nitrogen backfill.

6. Conduction accounts for 55 to 75% of the total heat transfer in the interior and 70 to 90% at the

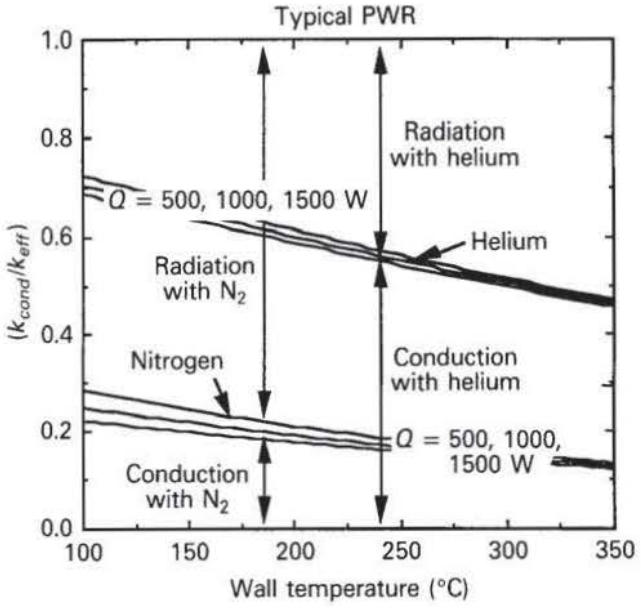

Fig. 21. Relative importance of conduction and radiation heat transfer in the interior region of a typical PWR assembly with either helium or nitrogen backfill.

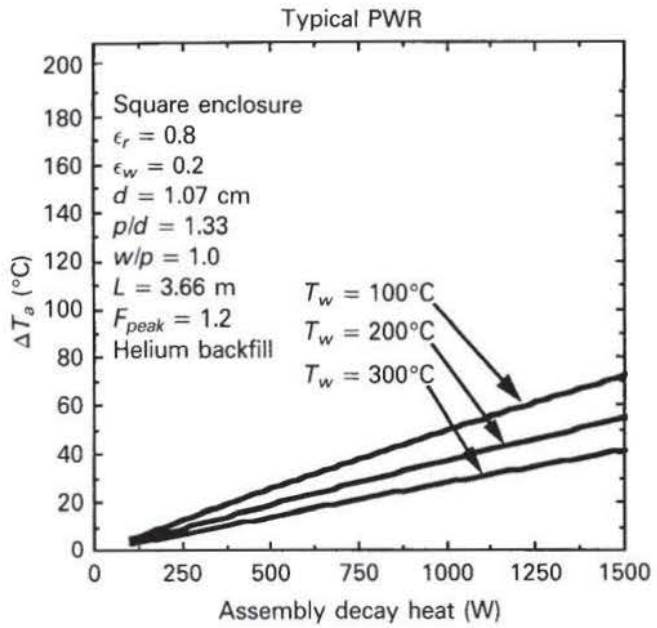

Fig. 20. Lumped k_{eff}/h_{edge} model predictions of ΔT_a for a typical PWR assembly with helium backfill.

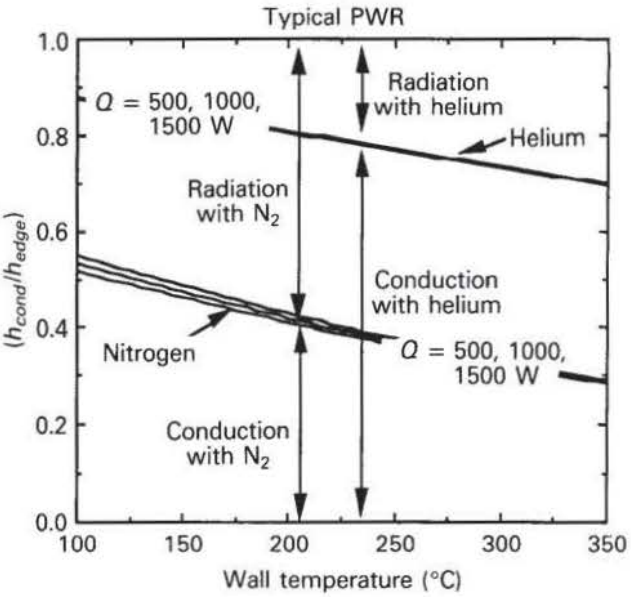

Fig. 22. Relative importance of conduction and radiation heat transfer at the edge region of a typical PWR assembly with either helium or nitrogen backfill.

edge of an enclosed PWR assembly with helium backfill.

The temperature drop at the edge ($T_e - T_w$) is compared with the total assembly temperature drop ($T_m - T_w$) in Fig. 23 for a typical PWR assembly. The general trends are as follows:

1. A significant fraction (25 to 50%) of the total temperature drop ($T_m - T_w$) is associated with the edge region ($T_e - T_w$) for both helium and nitrogen backfill.

2. Nitrogen backfill leads to a larger fraction (~45%) of the total temperature drop being associated with the edge region.

3. The fraction of the total temperature drop associated with the edge region is not significantly influenced by the value of the wall temperature.

4. Forty to fifty percent of the total assembly temperature drop is associated with the edge region for nitrogen backfill.

5. Twenty-five to thirty-five percent of the total assembly temperature drop is associated with the edge region for helium backfill.

The predictions generated by the lumped k_{eff}/h_{edge} model are compared with the Wooton-Epstein correlation[13] because the correlation has been and remains widely used in the industry (see Table I). The Wooton-Epstein correlation is similar to the lumped k_{eff}/h_{edge} equations in that it is a nonlinear algebraic equation. For a typical 15 × 15 PWR assembly, the Wooton-Epstein correlation is

$$q_w = \frac{C_1 \sigma}{\frac{1}{\epsilon_w} + \frac{1}{\epsilon_r} - 1} (T_m^4 - T_w^4) + C_2 (T_m - T_w)^{4/3} , \tag{33}$$

where

q_w = heat flux at the enclosure surface (W/m^2)

$C_1 = 0.234$ (dimensionless)

$C_2 = 0.815$ [W/(m^2·K$^{4/3}$)].

The Wooton-Epstein correlation is based on models of thermal radiation and turbulent convection (instead of stagnant-gas conduction) heat transfer. A concentric ring model for radiative heat transfer is used to relate the maximum temperature to the wall temperature. The convective coefficient [C_2 in Eq. (33)] was determined from experimental data by using an electrically simulated 17 × 17 rod array with air backfill.[13] The 4/3 exponent for ($T_m - T_w$) in Eq. (31) indicates that the natural convection was assumed to be turbulent.

The lumped k_{eff}/h_{edge} predictions (solid lines) are compared with the predictions generated by using the Wooton-Epstein correlation (dashed lines) in Fig. 24. As illustrated, the lumped k_{eff}/h_{edge} predictions agree with the correlation for the case of $T_w = 200$°C, which is approximately the range of experimental data used to generate the Wooton-Epstein correlation.[13] The solutions, however, increasingly differ for different wall

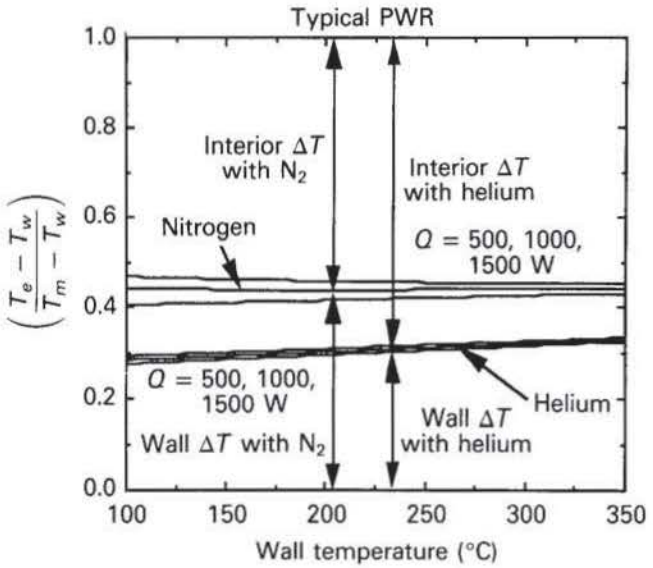

Fig. 23. Relative importance of the temperature drop associated with either the interior or wall region for a typical PWR assembly with either helium or nitrogen backfill.

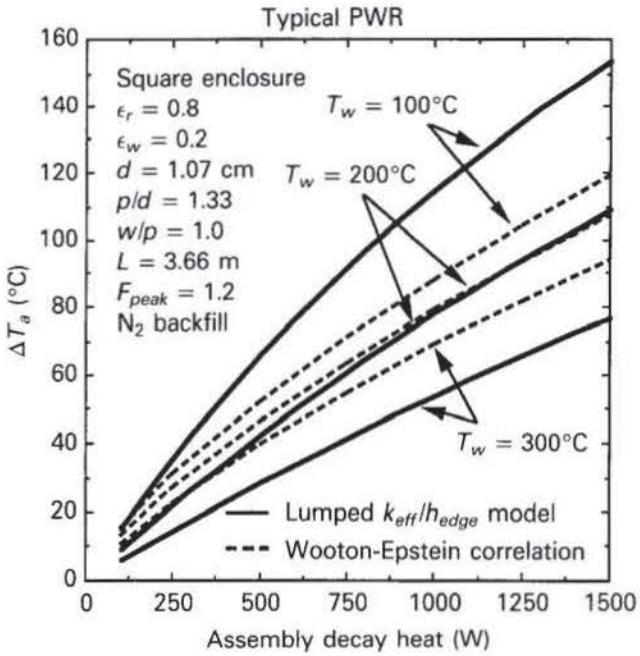

Fig. 24. Comparison of the lumped k_{eff}/h_{edge} model predictions (solid lines) and the Wooton-Epstein correlation (dashed lines) for a typical PWR assembly with nitrogen backfill.

temperatures. At $T_w = 300°C$, the Wooton-Epstein correlation overpredicts ΔT_a, and at $T_w = 100°C$, it underpredicts ΔT_a. Finally, the Wooton-Epstein correlation [Eq. (33)] and the plot of its predictions (dashed lines in Fig. 24) were presented with errors in Ref. 12, and the errors have been corrected in Refs. 44 and 45 and in this paper.

In comparison, the lumped k_{eff}/h_{edge} method is based on a more rigorous model of the governing heat transfer mechanisms and is proposed to yield more accurate predictions. In addition, the lumped k_{eff}/h_{edge} model has a much broader range of application in that it can accommodate different backfill gases, different array cross-sectional geometries, both square and hexagonal rod patterns, different rod diameters, different pitch-to-diameter ratios, and different wall-to-pitch ratios.

IV.B. Linear Algebraic Form of the Lumped k_{eff}/h_{edge} Model

Equations (26) and (27) may be simplified into the form of a single linear algebraic equation so that calculations may then be performed quickly without reliance on a computer. The linear solution will be shown to be conservative by overestimating ΔT_a (hence overestimating the maximum temperature). The linear equations are generated by linearizing the difference in the fourth powers of temperature in the radiative transfer term:

$$T_i^4 - T_j^4 \cong 4\left(\frac{T_i + T_j}{2}\right)^3 (T_i - T_j) \ , \tag{34}$$

where the subscripts i and j are used for generality.

One objective of linearization is to make Eqs. (26) and (27) appear as simple heat transfer equations that contain an effective conductivity term and an edge conductance term. In particular, Eq. (26) can be cast in the following form:

$$\frac{QF_{peak}}{SL_a} = k_{eff}(T_m - T_e) \ , \tag{35}$$

where the effective conductivity is defined in Eqs. (1), (2), and (14). Equation (35) can be manipulated to yield

$$T_m - T_e = R_{int} Q \tag{36}$$

with

$$R_{int} = \frac{F_{peak}}{SL_a k_{eff}} \ , \tag{37}$$

where R_{int} is the thermal resistance in the interior region of an assembly. The effective thermal conductivity is evaluated at the wall temperature, so that R_{int} can be evaluated to a constant value. This is considered an approximation, which leads to an underestimate of k_{eff} (because the wall temperature is always less than either the maximum or extrapolated temperatures), hence overprediction of T_m. Alternatively, Eq. (37) can be derived from Eq. (31) [instead of Eq. (26)], where it can be shown that $R_{int} = (C_1 + C_2 4T^3)^{-1}$.

Similarly, the edge model can be cast in the linear form as

$$\frac{QF_{peak}}{L_a L_c} = h_{edge}(T_e - T_w) \ , \tag{38}$$

where the edge conductance is defined in Eqs. (16), (17), and (19). Equation (38) can be manipulated to yield

$$T_e - T_w = R_{edge} Q \tag{39}$$

with

$$R_{edge} = \frac{F_{peak}}{L_a L_c h_{edge}} \ , \tag{40}$$

where R_{edge} is the thermal resistance at the edge region of an enclosed assembly. The edge conductance is evaluated at the wall temperature, so that R_{edge} can be evaluated to a constant value. Equation (40) can also be derived from Eq. (32) [instead of Eq. (27)], where it can be shown that $R_{edge} = (C_3 + C_4 4T^3)^{-1}$.

Equations (36) and (39) can be combined to eliminate T_e and yield one equation:

$$\Delta T_a = R_{total} Q \tag{41}$$

with

$$R_{tot} = R_{int} + R_{edge} \ , \tag{42}$$

where R_{tot} is the total thermal resistance for the enclosed spent-fuel assembly.

The interior, edge, and total thermal resistances have been calculated for a typical PWR and a typical BWR assembly, for both helium and nitrogen backfill and for three enclosure wall temperatures (100, 200, and 300°C). The results are summarized in Table III. Equation (41) overestimates ΔT_a compared with the solutions of Eqs. (31) and (32), and a comparison is shown in Fig. 25 for the PWR with nitrogen backfill. The linear solutions [from Eq. (41)] are straight lines that are coincident with the nonlinear solutions at the low assembly decay heat values and overshoot the nonlinear solutions at higher assembly decay heat values. The usefulness of the linear formulation of the k_{eff}/h_{edge} model is that the model can be used quickly to assess the ΔT_a without reliance on a computer.

V. CONCLUSIONS

The objective of this work was to develop a simple, accurate, defensible method to predict the maximum temperature of a spent-fuel assembly residing in an enclosure as encountered in shipping and transportation casks. An effective thermal conductivity and edge conductance model have been developed for both an interior and an edge region of the enclosed assembly. The

TABLE III

Coefficients in the Linear Form of the Lumped k_{eff}/h_{edge} Model* for a Typical PWR and a Typical BWR Spent-Fuel Assembly in Either Helium or Nitrogen Backfill with Enclosure Wall Temperature of Either 100, 200, or 300°C

	R_{int} (°C/kW)	R_{edge} (°C/kW)	R_{tot} (°C/kW)
Typical PWR[a] with helium backfill			
$T_w = 100$°C	41.8	13.1	54.9
$T_w = 200$°C	32.5	12.2	44.7
$T_w = 300$°C	24.3	11.0	35.3
Typical PWR with N_2 backfill			
$T_w = 100$°C	95.0	49.0	144.0
$T_w = 200$°C	57.7	36.3	94.0
$T_w = 300$°C	36.0	26.0	62.0
Typical BWR[b] with helium backfill			
$T_w = 100$°C	40.3	22.7	63.0
$T_w = 200$°C	30.7	21.0	51.7
$T_w = 300$°C	22.5	18.5	41.0
Typical BWR with N_2 backfill			
$T_w = 100$°C	87.4	82.0	169.4
$T_w = 200$°C	52.1	59.3	111.4
$T_w = 300$°C	32.2	41.5	73.7

*Equations (35) through (42).

[a]A typical PWR has an average design burnup of ~36 GWd/tonne U and ~0.46 tonne U so that the assembly decay heat after 10 yr cooling is ~0.562 kW. The maximum design burnup is ~50 GWd/tonne U (up to ~60 GWd/tonne U) so that the assembly decay heat after 10 yr cooling is ~0.856 kW (up to ~1.11 kW).

[b]A typical BWR has an average design burnup of ~30 GWd/tonne U and ~0.20 tonne U so that the assembly decay heat after 10 yr cooling is ~0.195 kW. The maximum design burnup is ~40 GWd/tonne U so that the assembly decay heat after 10 yr cooling is ~0.275 kW.

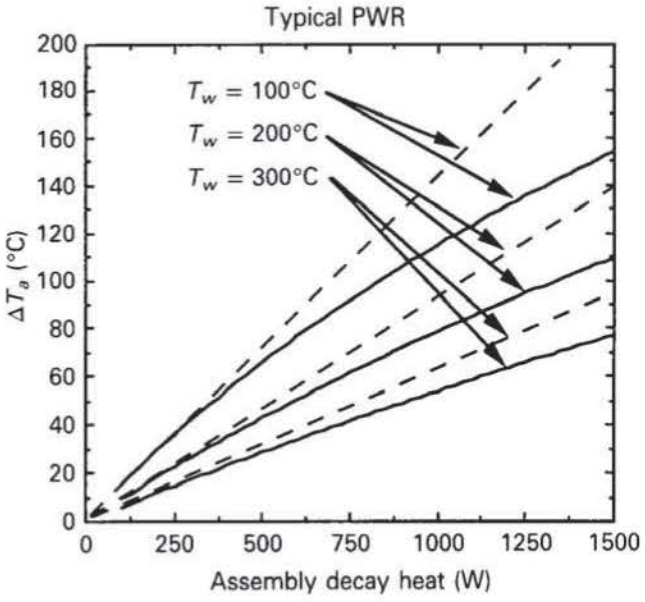

Fig. 25. Comparison of the linear lumped k_{eff}/h_{edge} model predictions [dashed lines, Eq. (41)] with the nonlinear lumped k_{eff}/h_{edge} model predictions [solid lines, Eqs. (31) and (32)] for a typical PWR assembly with nitrogen backfill.

models include conductive and radiative heat transfer. Convection heat transfer has a negligible effect on the value of the maximum temperature within an enclosed spent-fuel assembly for the vast majority of shipping and storage casks; hence, it is frequently neglected in the model. The lumped formulation of the k_{eff}/h_{edge} model was derived by solving the nonlinear heat diffusion equation within the interior region of an array. The lumped k_{eff}/h_{edge} model generates two coupled nonlinear algebraic equations relating the maximum, extrapolated, and wall temperatures.

The lumped k_{eff}/h_{edge} model has been validated by using data from five separate experiments. The model has been applied to a typical PWR and a typical BWR spent-fuel assembly with helium or nitrogen backfill where nonlinear algebraic equations are generated. The model predicts that the heat transfer due to conduction in an array interior ranges from 10 to 30% with nitrogen backfill and from 45 to 75% with helium backfill. The heat transfer due to conduction in the edge region ranged from 30 to 55% for nitrogen and 70 to 90% for helium. It was also noted that ~30% of the total assembly temperature drop is associated with the edge region for helium backfill, and 45% for nitrogen backfill.

The lumped k_{eff}/h_{edge} model was compared with the E-MAD correlation and the Wooton-Epstein correlation. These correlations have recently been used in the industry and represent the state of the art. Overall good agreement was reported for a large range of wall temperature and assembly decay heat values. A simplified linear form of the k_{eff}/h_{edge} model has been developed so that calculations may be performed quickly without reliance on a computer.

The benefits of the proposed k_{eff}/h_{edge} model is that it is just as easy (if not easier) to use as the previous correlations, and the proposed model is based on rigorous formulations of the governing heat transfer mechanisms. As such, the model is proposed to yield more accurate predictions for a larger range of assembly types, enclosure temperatures, and assembly decay powers.

ACKNOWLEDGMENTS

This work was originally performed at MIT with support by DOE through SNL under contract DE-AC04-76DP00789. This paper was prepared at the Center for Nuclear Waste Regulatory Analyses with support by the U.S. Nuclear Regulatory Commission (NRC) under contract NRC-02-88-005. This paper does not reflect the views or positions of either the DOE or NRC.

REFERENCES

1. "Preliminary Design Report B&W BR-100 100-Ton Rail/Barge Spent Fuel Shipping Cask," DOE/ID/12701, U.S. Department of Energy (1990).

2. "Preliminary Design Report for NAC Combined Transport Cask," DOE/ID/12702, U.S. Department of Energy (1990).

3. "TITAN Legal Weight Truck Cask Preliminary Design Report," DOE/ID/12699, U.S. Department of Energy (1990).

4. "GA-4/GA-9 Legal Weight Truck from Reactor Spent Fuel Shipping Casks," DOE/ID/12698, U.S. Department of Energy (1990).

5. "Packaging and Transportation of Radioactive Material," Code of Federal Regulations, Title 10, Part 71 (1992).

6. "Licensing Requirements for the Independent Storage of Spent Nuclear Fuel and High-Level Radioactive Waste," Code of Federal Regulations, Title 10, Part 72 (1992).

7. A. B. JOHNSON and E. R. GILBERT, "Technical Basis for Storage of Zircaloy-Clad Spent Fuel in Inert Gases," PNL-4835, Pacific Northwest Laboratory (1983).

8. M. W. SCHWARTZ and M. C. WITTE, "Spent Fuel Cladding Integrity During Dry Storage," UCID-21181, Lawrence Livermore National Laboratory (1987).

9. A. K. MILLER, M. GROOKS, T. Y. CHEUNG, A. TASOOJI, J. C. WOOK, J. R. KELM, B. A. SURETTE, and C. R. FROST, "Estimates of Zircaloy Integrity During Dry Storage of Spent Nuclear Fuel," EPRI-NP-6387, Electric Power Research Institute (1989).

10. W. H. LAKE, "Developing a New Generation of Spent Fuel Casks," *Proc. 9th Int. Symp. Packaging and Transportation of Radioactive Materials*, Washington, D.C., June 11–16, 1989, CONF-890631, Oak Ridge National Laboratory (1989).

11. W. H. LAKE, "Description of From-Reactor Transportation Cask Designs," *J. Inst. Nucl. Mater. Manage.*, **10**, 34 (1990).

12. R. D. MANTEUFEL, "Heat Transfer in an Enclosed Rod Array," PhD Thesis, Department of Mechanical Engineering, Massachusetts Institute of Technology (1991).

13. R. O. WOOTON and H. M. EPSTEIN, "Heat Transfer from a Parallel Rod Fuel Element in a Shipping Container," Unpublished Report, Battelle Memorial Institute (1963); see also J. A. BUCHOLZ, "Scoping Design Analyses for Optimized Shipping Casks Containing 1-, 2-, 3-, 5-, 7-, or 10-Year-Old PWR Spent Fuel," ORNL/CSD/TM-149, Appendix J, Oak Ridge National Laboratory (1983).

14. R. UNTERZUBER, R. D. MILNES, B. A. MARINKOVICH, and G. M. KUBANCSEK, "Spent-Fuel Dry-Storage Testing at E-MAD (March 1978 Through March 1982)," PNL-4533, Pacific Northwest Laboratory (1982).

15. J. S. WATSON, "Heat Transfer from Spent Reactor Fuels During Shipping: A Proposed Method for Predicting Temperature Distribution in Fuel Bundles and Comparison with Experimental Data," ORNL-3439, Oak Ridge National Laboratory (1963).

16. S. R. FIELDS, "STAFF-5, A Two-Dimensional Computer Model for Simulation of the Performance of Spent Fuel in Storage/Disposal," HEDL-TC-1601, Hanford Engineering Development Laboratory (1981).

17. C. A. RHODES, "COXPRO-II: A Computer Program for Calculating Radiation and Conduction Heat Transfer in Irradiated Fuel Assemblies," ORNL/TM-9000, Oak Ridge National Laboratory (1984).

18. L. E. FISCHER, "Spent Fuel Pin Temperature PC Code," UCRL-91019, Lawrence Livermore National Laboratory (1985).

19. D. R. RECTOR, C. L. WHEELER, and N. J. LOMBARDO, "Cobra-SFS: A Thermal-Hydraulic Analysis Computer Code," PNL-6049, Pacific Northwest Laboratory (1986).

20. M. KEYHANI, F. A. KULACKI, and R. N. CHRISTENSEN, "Heat Transfer Within Spent Fuel Canisters: Phase Two of an Experimental Laboratory Study," BMI/ONWI-530, Battelle Memorial Institute (1987).

21. R. A. McCANN, "HYDRA-II, A Computer Code for Hydrothermal Analysis of Spent Fuel Storage Systems," *Proc. Natl. Heat Transfer Conf.*, Houston, Texas, July 24–27, 1988, p. 149, H. R. JACOBS, Ed., American Society of Mechanical Engineers (1988).

22. L. E. FISCHER, "Spent Fuel Heating Analysis (SFHA) Code," UCRL-21711, Lawrence Livermore National Laboratory (1989).

23. G. L. JOHNSON and A. B. SHAPIRO, "SCANS (Shipping Cask Analysis System) A Microcomputer Based Analysis System for Shipping Cask Design Review Volume 4—Theory Manual Thermal Analysis," NUREG/CR-4554, U.S. Nuclear Regulatory Commission (1989).

24. M. W. WENDEL and G. E. GILES, "HTAS2: A Three-Dimensional Transient Shipping Cask Analysis Tool," NUREG/CR-5366, ORNL/CSD/TM-267, Oak Ridge National Laboratory (1990).

25. "SCDAP/RELAP5/MOD2 Code Manual, Volume 4: MATPRO—A Library of Materials Properties for Light-Water-Reactor Accident Analysis," NUREG/CR-5273, U.S. Nuclear Regulatory Commission (1990).

26. J. M. BATES, "Single PWR Spent Fuel Assembly Heat Transfer Data for Computer Code Evaluations," PNL-5571, Pacific Northwest Laboratory (1986).

27. R. A. McCANN, "Comparison of HYDRA Predictions to Temperature Data from Two Single-Assembly Spent Fuel Heat Transfer Tests," PNL-6074, Pacific Northwest Laboratory (1986).

28. N. J. LOMBARDO, T. E. MICHENER, C. L. WHEELER, and D. R. RECTOR, "Cobra-SFS Predictions of Single Assembly Spent Fuel Heat Transfer Data," PNL-5781, Pacific Northwest Laboratory (1986).

29. LORD RAYLEIGH, "On the Influence of Obstacles Arranged in Rectangular Order upon the Properties of a Medium," *Phil. Mag.*, **34**, *5*, 481 (1892).

30. R. D. MANTEUFEL and N. E. TODREAS, "Analytic Formulae for the Effective Conductivity of a Square or Hexagonal Array of Parallel Tubes," *Fundamental Problems in Conduction Heat Transfer*, HTD-207, p. 43, G. P. PETERSON and M. M. YOVANOVICH, Eds., American Society of Mechanical Engineers (1992)

31. "Characteristics of Spent Fuel, High-Level Waste, and Other Radioactive Wastes Which May Require Long-Term Isolation," DOE/RW-0184, U.S. Department of Energy (1987).

32. N. E. TODREAS and M. S. KAZIMI, *Nuclear Systems I: Thermal Hydraulic Fundamentals*, Hemisphere, New York (1990).

33. P. E. EGGERS, "Thermal Testing of Simulated BWR Consolidated Fuel," EPRI-NP-4119, Electric Power Research Institute (1985).

34. L. C. SANCHEZ and M. L. HUDSON, "Determination of Effective Thermal Conductivities for a Full-Scale Mock-Up of a 217-Element Breeder Reactor Fuel Assembly Subjected to Normal Shipping Conditions," SAND85-2827, Sandia National Laboratories (1986).

35. P. M. LOVETT, "An Experiment to Simulate the Heat Transfer Properties of a Dry Horizontal Spent Nuclear Fuel Assembly," MS Thesis, Department of Nuclear Engineering, Massachusetts Institute of Technology (1991).

36. G. E. DRIESEN, D. F. MORAN, P. S. SHERBA, and R. J. STEFFEN, "Heat Transfer Associated with Dry Storage of Spent LWR Fuel," *Heat Transfer in Nuclear Waste Disposal*, HTD-11, p. 9, F. A. KULACKI and R. W. LYCZKOWSKI, Eds., American Society of Mechanical Engineers, New York (1980).

37. J. B. WRIGHT and H. H. IRBY, "An Overview of Dry Interim Storage Research and Development Activities at the E-MAD Facility, Nevada Test Site," *Proc. Int. Workshop Irradiated Fuel Storage: Operating Experience and Development Programs*, S. J. NAQVI and C. R. FROST, Eds., Ontario Hydro (1984).

38. M. A. GOTOVSKY, E. D. FEDOROVICH, V. N. FROMZEL, and V. A. SHLEIFER, "Heat Transfer of Rod Bundle in Closed Volume Filled with Gas," *Heat Exchange in Atomic Power Plants Energy Equipment*, p. 76, S. N. TRUDOV, Ed., Science (Nauka), Leningrad (1986) (in Russian).

39. N. V. VDOVETS, A. I. GRIVNIN, M. A. GOTOVSKY, T. A. PERVITSKAYA, V. N. FROMZEL, E. D. FEDOROVICH, and V. A. SHLEIFER, "Natural-Convection Heat Transfer in Horizontal Bundles of Fuel Rods," *High Temperature*, **24**, *4*, 545 (1986).

40. J. Y. HWANG and L. E. EGGERDING, "Thermal Analysis Design and Experimental Evaluation of a Prototype Spent Fuel Dry Storage Cask," *Proc. ANS/ASME Nuclear Power Conf.*, p. 165, American Society of Mechanical Engineers (1988).

41. J. Y. HWANG and L. E. EGGERDING, "Development of a Thermal Analysis Model for a Nuclear Spent Fuel Storage Cask and Experimental Verification with Prototype Testing," *ASME J. Eng. Gas Turbines and Power*, **111**, 647 (1989).

42. J. M. CUTA and J. M. CREER, "Comparisons of COBRA-SFS Calculations with Data from Simulated Sections of Unconsolidated and Consolidated BWR Spent Fuel," EPRI-NP-4593, Electric Power Research Institute (1986).

43. S. WOLFRAM, *Mathematica, A System for Doing Mathematics by Computer*, Addison-Wesley, Redwood, California (1988).

44. R. D. MANTEUFEL and N. E. TODREAS, "Heat Transfer in an Enclosed Rod Array," MITNE-292, Department of Nuclear Engineering, Massachusetts Institute of Technology (1991).

45. R. D. MANTEUFEL and N. E. TODREAS, "Effective Thermal Conductivity and Edge Conductance Model for a Standard PWR Spent-Fuel Assembly," *Trans. Am. Nucl. Soc.*, **65**, 65 (1992).

Randall D. Manteufel [BS, engineering science, University of Texas at Austin, 1984; MS, mechanical engineering, University of Texas at Austin, 1987; PhD, mechanical engineering, Massachusetts Institute of Technology (MIT), 1991] is a research engineer at the Center for Nuclear Waste Regulatory Analyses at Southwest Research Institute. His main interests are in heat and mass transfer with application to radioactive waste management. He is currently active in the areas of performance assessment, thermohydrology, and coupled processes in the support of the U.S. high-level radioactive waste program.

Neil E. Todreas (BS and MS, mechanical engineering, Cornell University, 1958; ScD, nuclear engineering, MIT, 1966) is the KEPCO Professor of Nuclear Engineering and a professor of mechanical engineering at MIT. His technical activities are focused on thermal-hydraulic aspects of nuclear system performance under steady-state and accident conditions.